Modeling Oil Spilling on Water

by

Guangyu Hui

Copyright © Guangyu Hui 2019

A Dissertation Submitted to the Faculty of the

Graduate Interdisciplinary Program in Applied Mathematics

In Partial Fulfillment of the Requirements
For the Degree of

Doctor of Philosophy

In the Graduate College

The University of Arizona

2 0 1 9

THE UNIVERSITY OF ARIZONA
GRADUATE COLLEGE

As members of the Dissertation Committee, we certify that we have read the dissertation prepared by *Guangyu Hui*, titled *Modeling Oil Spilling on Water* and recommend that it be accepted as fulfilling the dissertation requirement for the Degree of Doctor of Philosophy.

Shankar C Venkataramani Date: 5/7/19

Kevin Lin Date: 5/7/19

Matthias Morzfeld Date: 5/8/19

Moysey Brio Date: 5-8-19

Final approval and acceptance of this dissertation is contingent upon the candidate's submission of the final copies of the dissertation to the Graduate College.

I hereby certify that I have read this dissertation prepared under my direction and recommend that it be accepted as fulfilling the dissertation requirement.

Shankar C Venkataramani Date: 5/7/19
Dissertation Committee Chair
Department of Mathematics, The University of Arizona

THE UNIVERSITY OF ARIZONA ®

Statement by Author

This dissertation has been submitted in partial fulfillment of requirements for an advanced degree at The University of Arizona and is deposited in the University Library to be made available to borrowers under rules of the Library.

Brief quotations from this dissertation are allowable without special permission, provided that accurate acknowledgment of source is made. Requests for permission for extended quotation from or reproduction of this manuscript in whole or in part may be granted by the copyright holder.

Signed:  Guangyu Hui 6/22/2019

Acknowledgements

At the conclusion point of my graduate study, I would like to thank many people that have supported me throughout.

First and foremost, I must thank my advisor Dr. Shankar Venkataramani for his unconditional support through my entire graduate path. This dissertation work cannot be accomplished without the help from him. Dr. Venkataramani not only offers me his generous advise in academic, but also his personality that always ready to help others has inspired me.

I would also like to thank the rest of my committee members. Many thanks to Dr. Matthias Morzfeld, who taught me data assimilation methods and provided a plenty of useful suggestions on my project. Thanks to Dr. Moysey Brio and Dr. Kevin Lin for their generous advise on the numerical methods and other aspects of the dissertation.

I am grateful for the help from Dr. Patrick Shipman, who is my undergraduate advisor and inspires my interest in applied mathematics.

My thanks also go to Stacey LaBorde and Keri Oligmueller who have arranged all administrative stuffs, especially my visa issues properly for me.

There are a few more people I have to mention, Dr. Hermann Flaschka, Dr. Bin Dong, Dr. Michael Tabor, Dr. Janek Wehr. Without the help from any of them, my path would have been more difficult.

Dedication

To my wife, Yanling Qiao and our daughter, Lauren Hui.

Table of Contents

Table of Contents—*Continued*

List of Figures

List of Tables

Abstract

For the offshore oil industry, a primary concern is an accidental oil spill. Potentially, oil can spill from the platform during the extraction or from the tanker during the transportation, in both cases will flow into the nearby sea. After an oil spill occurs, to prevent it from polluting even more areas and recover the polluted area, scientists want to understand the process of oil spreading on the sea.

In this dissertation, we study the phenomena of oil spreading on water surface. We address a reduced model that captures the local dynamics of an oil slick spreading on flowing water surface and provides an insight on the trend of the spreading process. When the underlying water is locally steady, a full PDE model is analyzed to yield the velocity of the oil slick and its spreading rate. For spreading on a water surface where the flow is locally contracting towards the center of the oil slick, a stationary state is found for the oil slick. For an oil slick spreading on a water surface where the flow is locally expanding towards the edge the slick, the asymptotic spreading rate of the slick and a quasi-steady state are found in this case. We also develop numerical schemes that simulate the dynamics of an oil slick spreading on steady water surface and surface with expanding water flow.

For modeling the evolution of crude oil, we introduce a dimension reduction for systems with slow relaxation and develop a multilayer stochastic model. Using the multilayer reduced model, we are able to estimate a single observable quantity of oil based on its past states, without further knowledge on the 'microscopic structure' inside the crude oil. Through synthetic data experiments, our reduced model is demonstrated to have an improved accuracy when implemented with data assimilation methods and can maintain stability while predicting a future state when no data is available.

Chapter 1

Introduction

Oil has been the most important fossil fuel for modern world since the early 20th century. Thanks to its massive storage in nature and high combustion efficiency, crude oil is the raw material for a wide variety of petroleum products that are used both in industry and daily life. It is estimated that the world consumes at least 96 million barrels of crude oil each day. About 40 percent of total energy consumption in the United States is made up by petroleum. By 2004, the world total explored reserve of oil is about 170 billion tons, among which about 24% is under the seabed. The scale of oil exploitation on the sea has increased dramatically since the first offshore oil platform was launched on the sea near the coast of California in 1896. Nowadays, more than 25% of the oil extracted each day is from offshore platforms. For the offshore oil industry, a primary concern is an accidental oil spill. Potentially, oil can spill from the platform during the extraction or from the tanker during the transportation, in both cases will flow into the nearby sea. Such industrial accidents have occurred dozens of times in the past few decades and have caused tremendous disasters and irreparable damage to a large scale oceanic ecosystem. Oil spills at sea can spread for hundreds of nautical miles in a thin oil slick which can cover beaches with a coating of oil and kill seabirds, mammals, shellfish and other organisms they coat. The Deepwater Horizon oil spills, also referred to as the BP oil spills in 2010, leaked an estimated total volume of 210 million gallons of oil into the Gulf of Mexico. According to the satellite image, the spill directly affect 68,000 square miles of ocean, which is comparable to the size of Oklahoma. About 491 miles of coastlines in Louisiana, Mississippi, Alabama and Florida were contaminated by oil two months after the spill is discovered. This accident is one of the worst industrial disasters in history and has brought the society a serious attention in the risk of oil spill.

After an oil spill occurs, to prevent it from polluting even more areas and recover the polluted area, scientists want to understand the process of oil spreading on the sea. The actual process of oil spilling on the sea is complicated. It consists of many different physical processes schematically, shown in Figure 1.2 [11]. The spread of an oil slick on the sea can be affected by many factors, including transport driven by winds and currents, dispersion of the floating oil layer into suspending oil bulks, dissolution of oil particles into water, evaporation of oil into air, and the tendency of the oil slick to spread even in calm water. Understanding the dynamics of the spreading process is even more challenging for crude oil, since crude oil is a mixture of a large number of chemical compounds, each with its own properties. Due to possible

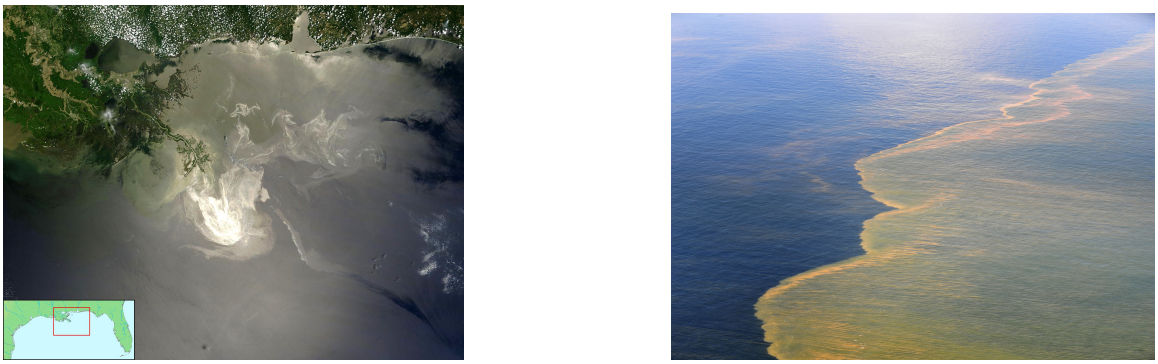

(a) (b)

Figure 1.1: (a) NASA's Terra Satellites Sees the Deepwater Horizon oil Spill on May 24 Sunlight illuminated the lingering oil slick off the Mississippi Delta on May 24, 2010. (b) Oil from the Deepwater Horizon oil spill approaches the coast of Mobile, Alabama, 6 May 2010. Captured from `https://en.wikipedia.org/wiki/Deepwater_Horizon_oil_spill`

chemical reactions between different components, also evaporation and dissolution, crude oil is in evolution during its spreading and its properties such as density and viscosity vary over time and space. Thus, it is difficult to model such a spilling process mathematically with consideration of all physical aspects.

Physicists have been studying the phenomenon of oil spreading on water both theoretically and experimentally since 1960's. Fay [8, 9] and Hoult [14] both derive an approximation of the spreading rate for a pure oil slick to spread on steady water surface. Buckmaster comes out an improved spreading law for the oil in calm water in a more dedicated time scale [2]. For effects other than spreading, Hoult estimates the wind driven velocity acting on the water surface and argued that the effect of waves would be small in this spreading process because of the small vertical acceleration and a nearly periodic behaviour of the ocean waves [14]. Chebbi gives an experimental study on the spread of oil under the gravity and viscous drag for the case where oil is discharged at a constant rate on calm water surface [4]. The experimental results justifies Hoult's analysis and further yield the prefactor for the spreading expression. Chebbi also extends and modifies the Fannelop & Waldman boundary condition to account for the case of continuous discharge of oil under the gravity and inertial effects, based on the analogy with the acoustic limit in gas dynamics [3]. Restrepo, Venkataramani and Dawson develop a physical model that studies the transport of floating oil in the nearshore [23]. To model the uncertainty quantification of crude oil, Venkataramani, Venkataramani and Restrepo develop a reduced stochastic model that tracks the evolution of crude oil using observable quantities [27].

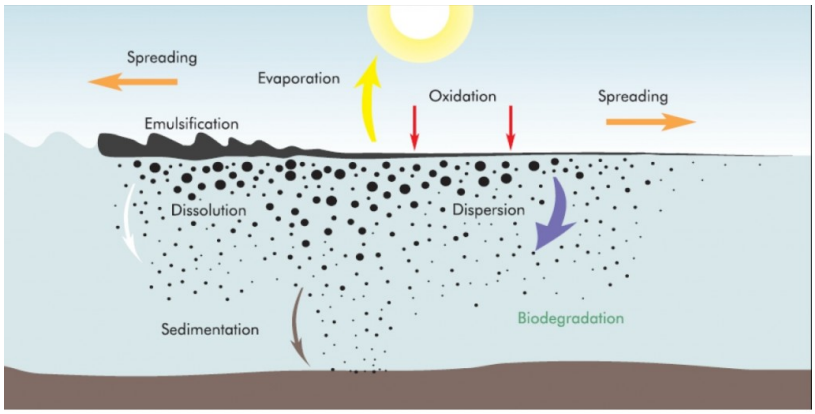

Figure 1.2: Physical effects that are evolved in oil spill process. Captured from `www.medess4ms.eu/marine-pollution`

1.1 Overall Goal

Due to the interactions of many physical processes, the dynamics of the oil spilling on water is complicated. Developing a full mathematical model that takes every aspect of the physics into account is difficult, even analyzing and applying such a multiphysics and multiscales model will be a challenge. In our work, we are aiming to develop a reduced model that not only captures the main dynamics of the oil spilling process, but also can be implemented in a practical way without further attentions on the details of every physical aspect.

1.2 Summary of Results

As a progress towards the overall goal, we have achieved four main results in this thesis:

1. A reduced model has been established for the oil spreading process on water.
2. A numerical solver has been developed to simulate the dynamics of an oil spreading on water and can be used to validate the reduced model.
3. The implementation of data assimilation methods on a reduced model for oil evaporation process has been investigated.
4. An improved reduced model for oil evaporation process has been developed to maintain accuracy and stability.

In this thesis, we will present our results through discussions on the following topics:

- The motivation of the reduced model for oil spreading on water
- Oil spreading on water surface with contracting flow
- A scale solution at the steady state for the contracting flow case
- A form of the analytic solution at the steady state for the contracting flow case
- A reduced ODE for the steady state solution for the contracting flow case
- Boundary conditions for the reduced ODE
- Numerical solutions of the reduced ODE
- Oil spreading on water surface with expanding flow
- A scale solution for the expanding flow case
- A full PDE model for the expanding flow case
- A form of the quasi-steady state solution for the expanding flow case
- A reduced ODE and its boundary conditions for the quasi-steady state solution
- Numerical solutions of the reduced ODE
- Implementation of Ensemble Kalman filter on a multilayer stochastic model for oil evaporation process
- Instability of the six taps multilayer model
- Estimation accuracy of the one tap multilayer model
- Derivation of the one tap model with multiple bins approach
- Comparison of six taps model, one tap model and one tap model with bins approach
- Limitation of the reduced model

1.3 Thesis Organization

This thesis is organized in the following order:

- In Chapter 2, from section 2.1, we review an order of magnitude analysis and a PDE model for an oil slick spreading on calm water.
- In Chapter 2, section 2.2, we review a dimension reduction for system with slow relaxation.
- In Chapter 3, we address a reduced model for an oil slick spreading on flowing water. We discuss the solution behaviors for scenarios with different water flows and develop a numerical solver to simulate the dynamics.
- In Chapter 4, we investigate the performance of the reduced model in estimating the oil evaporation process and discuss the influence of noise from the data. We develop an advanced reduced model that improves the prediction stability and discuss the limitation of data assimilation implementation in this application.

Chapter 2

Background

2.1 Fluid Dynamics of An Oil Slick On Steady Water

In this section, we will explore the dynamics of an oil slick spreading on steady water surface.

2.1.1 A Order of Magnitude Analysis

Fay [8, 9] firstly developed an estimation on the rate of spread of an oil slick in calm water using the order-of-magnitude analysis in 1969. The result are based on several assumptions in the following.

1. A hydrostatic equilibrium is assumed for the oil slick due to the fact that oil layer is typically very thin, comparing to its horizontal scale and the wavelength of the waves underneath it.

2. A bulk model that assumes constant chemical properties for the oil slick is used by Fay.

It is noted that for crude oil, since different chemical compounds generally have quite different spreading coefficients due to surface tension, such a bulk model assumption may be a rather poor description of the flow in a regime where surface-tension and viscous effects are important. We will address a statistical framework that can be implemented to improve this problem in later sections.

Referring to Fay's analysis, let us consider an one-dimensional setting where the oil is spreading unidirectionally on the water surface, illustrated in Figure 2.1. With the bulk model assumption, there are four basic forces that either promote or retard the spreading of the oil slick, which are the gravitational force, the inertial force, the viscous drag and surface tension. We will use l to represent the characteristic

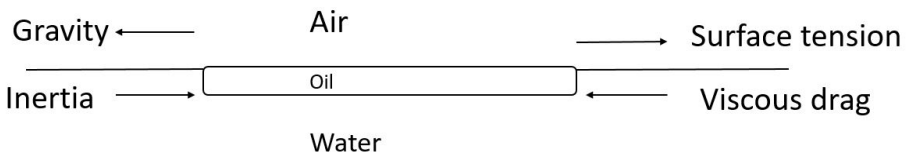

Figure 2.1: Oil slick on water

length scale of the oil layer, h to represent the characteristic thickness scale of the oil layer, and t to represent the characteristic time scale of the dynamics. Assume that water has kinematic viscosity ν_w, oil has kinematic viscosity ν_o and the relative density difference between water and oil is Δ, i.e. $\rho_{oil} = \rho_{water}(1 - \Delta)$. Typically, $\nu_w \ll \nu_o$ and Δ is so small (usually $\Delta \leq 0.1$) that we will only consider the density difference when evaluating the gravitational force. Then the orders of magnitude of these promoting and retarding forces can be estimated by the characteristics in the following way.

Because of the hydrostatic equilibrium in the oil, the oil slick floats a height Δh above the mean water surface, which generates a pressure of the order

$$\rho g \Delta h$$

resulting in a horizontal gravitational driving force that has a order of

$$\rho g \Delta h h \tag{2.1.1}$$

While an oil slick is released from the rest, the inertia effect tends to retard the motion. The order of such a inertial force is given by the Newton's law

$$\rho l t^{-2}(hl) \tag{2.1.2}$$

As the oil is much more viscous than water, while it sliding over the water surface, a water boundary layer is formed. The Blasius solution [12] provides an approximation of the thickness δ of a laminar boundary layer

$$\delta \approx 5.0\sqrt{\frac{\nu_w x}{u_0}}$$

Using this solution as the thickness of the boundary layer, the order of the viscous drag can be estimated by

$$\rho \nu_w l t^{-1}(\nu_w t)^{-\frac{1}{2}} l \tag{2.1.3}$$

While the slick is spreading on water, multiple surface tensions result from the air, water and oil interfaces can act on the edge. We will only characterize the net surface tension defined as

$$\sigma = \sigma_1 - \sigma_2 - \sigma_3 \tag{2.1.4}$$

where σ_1 is the air-water interfacial tension, σ_2 is the oil-water interfacial tension, and σ_3 is the oil-air interfacial tension. In general, the effect of the surface tension to either promote or retard the spreading is determined by the sign of σ. For most crude oils, the net surface tension is measured to be positive [14] so that it will promote the spreading.

Now suppose an oil slick with a constant volume V is released at a point and starts spreading on the water surface. An estimation on the order of characteristic length scale gives

$$hl \sim V$$

The inertial force and viscous drag tend to retard the oil. For a very short period of time after the release, the oil layer is relatively thick so that the inertial force dominates the viscous drag as the main retarding force. More precisely, by comparing the orders of magnitude of these two retarding forces, we can see that

$$\rho\nu_w lt^{-1}(\nu_w t)^{-\frac{1}{2}}l \ll \rho lt^{-2}(hl) \tag{2.1.5}$$

when

$$t \ll \nu_w^{-1}h^2 \tag{2.1.6}$$

For the promoting side, the gravitational force dominates surface tension as the main driving force, when the oil layer is thick. In particular,

$$\rho g\Delta hh \gg \sigma, \tag{2.1.7}$$

when

$$h \gg (\frac{\sigma}{\rho g\Delta})^{\frac{1}{2}} \tag{2.1.8}$$

Thus for a short period of time after the oil slick is released when the thickness of the oil layer is still relatively thick, the gravitational force and the inertial force are the dominating promoting and retarding forces, respectively. We will refer this stage of dynamics as the 'Inertial' regime. A rough spreading law for this regime can be obtained by balancing the orders of the gravitational force and the inertial force:

$$\begin{aligned} &\rho(lt^{-2})hl \sim \rho g\Delta hh \\ &\Rightarrow l \sim (g\Delta V)^{\frac{1}{3}}t^{\frac{2}{3}} \end{aligned} \tag{2.1.9}$$

Substituting the spreading law (2.1.9) into (2.1.6) and making use of the fact $hl \sim V$ yields the time scale for this regime:

$$t \ll (g\Delta)^{-\frac{2}{7}}V^{\frac{4}{7}}\nu_w^{-\frac{3}{7}} \tag{2.1.10}$$

It is noted that the upper bound of the time scale for this regime increases with the volume of the oil slick. Intuitively, this can be explained by the reason that it takes longer for a large amount of oil to spread out as an oil layer that is reasonably thin.

After certain amount of time, the oil slick is spreading out and becomes to a thin layer. Once the layer thickness is thin enough, it is expected that the viscous drag starts dominating the inertial force as the main retarding effect. Referring to (2.1.6), this scenario happens when

$$t \gg \nu_w^{-1} h^2$$

or equivalently

$$(\nu_w t)^{\frac{1}{2}} \gg h \tag{2.1.11}$$

which means when the boundary layer thickness is much larger than the thickness of the oil layer. On the other hand, we should not forget that the boundary layer description of the water flow is only appropriate if the Reynolds number is large, which implies that

$$(\nu t)^{\frac{1}{2}} \ll l \tag{2.1.12}$$

On the promoting effect side, let's assume that the oil layer is not thin enough so that the inequality (2.1.8) still holds, which indicates that the gravitational force still dominates the surface tension. We will refer this stage of the dynamics as the 'Viscous' regime. A balance on the orders of magnitude of the viscous drag and the gravitational force yields an estimation of the spreading law of this regime:

$$\begin{aligned} &\rho \nu_w l t^{-1} (\nu_w t)^{-\frac{1}{2}} l \sim \rho g \Delta h h \\ &\Rightarrow l \sim t^{\frac{3}{8}} (gV)^{\frac{1}{4}} V^{\frac{1}{2}} \nu_w^{-\frac{1}{8}} \end{aligned} \tag{2.1.13}$$

The bounds of the time scale for this regime are given by (2.1.12) and (2.1.8). By substituting the spreading law (2.1.13) into (2.1.12) and (2.1.8), we obtain the time scale for the 'Viscous' regime:

$$(g\Delta)^{-\frac{2}{7}} V^{\frac{4}{7}} \nu_w^{-\frac{3}{7}} \ll t \ll (g\Delta)^2 V^4 \nu_w^{-5} \tag{2.1.14}$$

Comparing to the upper bound of the time scale for the 'Inertial' regime, the upper bound of the time scale for this 'Viscous' regime increases much faster with the volume of the oil ($\sim V^4$). Thus for a large volume of oil spills, we expect the spreading dynamics stays in this 'Viscous' regime much longer than in the 'Inertial' regime.

At the last stage of spreading, after a long period of time, the oil layer becomes extremely thin ($h \sim 0$) so that the viscous drag is dominating the inertial force as the main retarding effect, while the surface tension is dominating the gravitational force as the main promoting effect. We will refer this stage of dynamics as the

Regime	Time Scale	Spreading Law
Inertial Regime	$t \ll (g\Delta)^{-\frac{2}{7}} V^{\frac{4}{7}} \nu_w^{-\frac{3}{7}}$	$l \sim (g\Delta V)^{\frac{1}{3}} t^{\frac{2}{3}}$
Viscous Regime	$(g\Delta)^{-\frac{2}{7}} V^{\frac{4}{7}} \nu_w^{-\frac{3}{7}} \ll t \ll (g\Delta)^2 V^4 \nu_w^{-5}$	$l \sim t^{\frac{3}{8}} (gV)^{\frac{1}{4}} V^{\frac{1}{2}} \nu_w^{-\frac{1}{8}}$
Surface Tension Regime	$t \gg (g\Delta)^2 V^4 \nu_w^{-5}$	$l \sim \sigma^{\frac{1}{2}} \rho^{-\frac{1}{2}} \nu_w^{-\frac{1}{4}} t^{\frac{3}{4}}$

Table 2.1: Oil Spreading Regimes

Parameter	Notation	Typical value
Volume of oil spills	V	$100 \sim 10000$ tonnes
Density of crude oil	ρ_{oil}	$870 \sim 920\ kg/m^3$
Density of sea water	ρ_{water}	$1025\ kg/m^3$
Fractional density difference	Δ	0.10∼0.15
Viscosity of oil	ν_{oil}	$326.87 \times 10^{-6} m^2/s$
Viscosity of water	ν_w	$1.004 \times 10^{-6} m^2/s$
Net surface tension	σ	$0.025 N/m$
Gravitational acceleration	g	$9.8\ m/s^2$

Table 2.2: Oil parameters

'Surface-Tension' regime. Again, an estimated spreading law for this regime comes from balancing the dominating forces from the promoting and retarding side:

$$\begin{aligned} &\rho \nu_w l t^{-1} (\nu_w t)^{-\frac{1}{2}} l \sim \sigma \\ &\Rightarrow l \sim \sigma^{\frac{1}{2}} \rho^{-\frac{1}{2}} \nu_w^{-\frac{1}{4}} t^{\frac{3}{4}} \end{aligned} \tag{2.1.15}$$

We note that in this regime, the spreading rate is independent of the oil slick's volume V, meaning that every oil slick that is spreading on the water surface, regardless of its size, will spread as $t^{\frac{3}{4}}$ eventually.

We summarize the three different regimes of the oil spreading dynamics in Table 2.1. Also, to have an intuition on how long each regime would be in a real oil spreading scenario, we list the natural values of the parameters that are involved in the order of magnitude analysis in Table 2.2. We then compute the time scales for each regime based on the parameter values listed and plot the estimated spreading law in Figure 2.2. For an oil spilling accident that spills hundreds of tonnes of oil on the ocean, the first 'Inertial' regime may last from couple of hours to one day, and the second 'Viscous' regime could last from several days to a month.

By the order-of-magnitude analysis above, one can get an estimation on the spreading rates in each stage of the dynamics and understand the manner of their dependence on the oil parameters. However, the actual spreading coefficients cannot be deduced from the order of magnitude estimates. To derive a more detailed spreading law for the oil spreading dynamics, a differential equation model is needed to describe

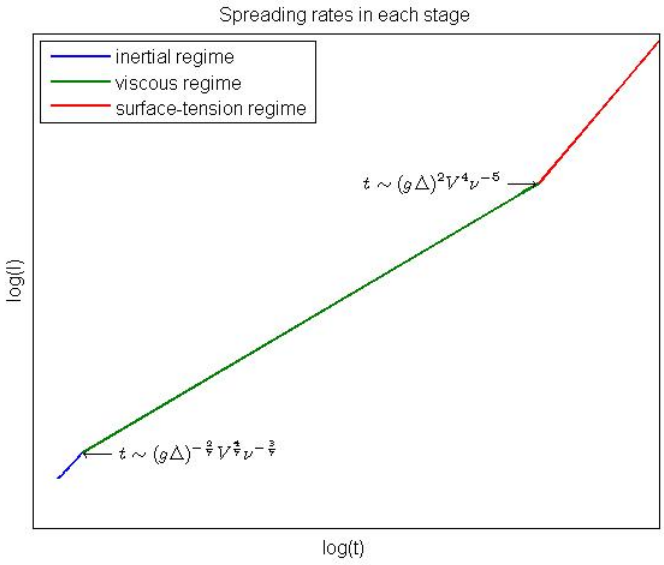

Figure 2.2: Oil spreading rates in each regime

the dynamics more precisely. Buckmaster firstly developed a PDE model that governs the dynamics of the oil spreading in 'Viscous' regime and derived a numerical spreading law from the model in 1973 [2]. We will review Buckmaster's solution in Section 2.2.

2.1.2 A PDE Model for The Viscous Regime of Oil Spreading

Let's first set up a coordinate system as shown in Figure 2.3, in which the origin was set at the center of the slick and the spreading of the slick is symmetric about the y-axis. In this section, we are going to explore the dynamics of the oil spreading in the 'Viscous' regime, whose time scale takes a major part of the entire spreading process. In this regime, the gravitational force from the oil slick is promoting its spreading and the viscous drag from the water is retarding the spreading.

Assume that the oil slick has width $2R(t)$, where

$$R(t) = Ct^{\alpha} \tag{2.1.16}$$

As suggested by the order of magnitude analysis (2.1.13), the spreading rate α should be equal to $\frac{3}{8}$, and this should also comes from the analysis of a dynamical model. Furthermore, the dependence of C on the flow parameters is also given by (2.1.13), but the actual spreading coefficients is not clear so far.

Because of a hydrostatic balance, the oil slick can be characterized by a velocity $q(x,t)$ that only varies horizontally, and a thickness $h(x,t)$. Thus the oil continuity

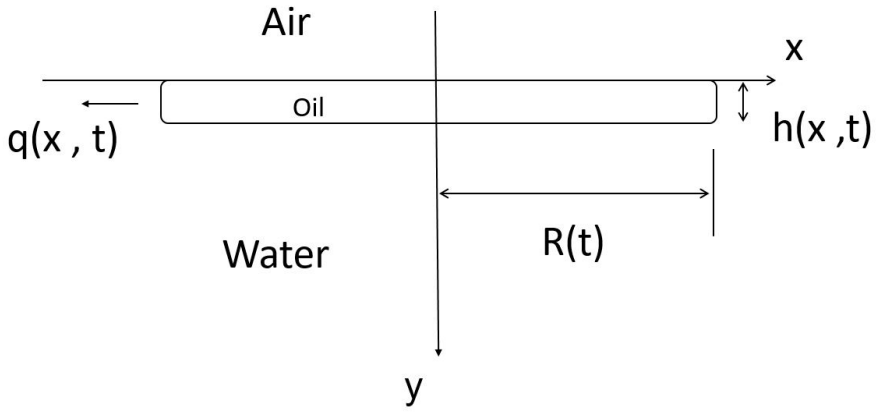

Figure 2.3: Frame setup at the center of oil slick

equation is

$$\frac{\partial h}{\partial t} + \frac{\partial (qh)}{\partial x} = 0 \tag{2.1.17}$$

The gravitational forces generate a horizontal pressure gradient in the oil, which drives its spreading. The force associated with this is balanced by the shear stress acting at the oil-water interface due to the water boundary layer. Suppose the water flow has velocities u, v in the horizontal and vertical direction, respectively. Then the momentum equation for the oil is written as

$$-\frac{\nu}{g\Delta}\frac{\partial u}{\partial y}(x, 0; t) + h\frac{\partial h}{\partial x} = 0 \tag{2.1.18}$$

As for the water flow, it is governed by the unsteady boundary-layer equations

$$\frac{\partial \mathbf{u}}{\partial t} + \mathbf{u} \cdot \nabla \mathbf{u} - \nu_w \Delta \mathbf{u} = -\nabla p \tag{2.1.19}$$

$$\nabla \cdot \mathbf{u} = 0 \tag{2.1.20}$$

A simplified equation that ignores the pressure divergence is used for the steady water case

$$\frac{\partial u}{\partial t} + u\frac{\partial u}{\partial x} + v\frac{\partial u}{\partial y} = \nu_w \frac{\partial^2 u}{\partial y^2} \tag{2.1.21}$$

$$\frac{\partial u}{\partial x} + \frac{\partial v}{\partial y} = 0 \tag{2.1.22}$$

The equation system is completed by certain boundary conditions. At the water-oil interface, a 'no-slip' boundary condition is assumed, i.e.

$$v(x,0;t)=0, \quad u(x,0;t)=q(x,t) \tag{2.1.23}$$

and, if the water is at the rest far from the oil-water interface,

$$\lim_{y\to\infty} u(x,y;t)=0 \tag{2.1.24}$$

In addition there is symmetry about the y axis, and with the assumption (2.1.16), at the edge of the slick q is equal to the edge velocity, i.e.

$$q(R(t),t)=\dot{R}(t) \tag{2.1.25}$$

With these boundary conditions, the problem description is complete. We now describe the procedure that Buckmaster follows to solve for the prefactor C in (2.1.16)[2]. Suppose that the velocity of the oil $q(x,t)$ is a known function of x and t, then the water boundary layer-equations (2.1.21),(2.1.22) can be solved with the boundary conditions (2.1.23),(2.1.24),(2.1.25). Once the water velocity $u(x,y;t)$ is obtained, the skin friction at the water-oil interface $\frac{\partial u}{\partial y}(x,0;t)$ is computable. Then we can integrate equation (2.1.18) to get the oil thickness $h(x,t)$. It is noted that the oil continuity equation (2.1.17) will only be satisfied if the $q(x,t)$ is picked correctly in the beginning. Once such a self-consistent solution is found, by integrating the thickness h, we will have the volume of the slick, which indicates the constant C.

Let's begin solving the boundary-layer equation near the center of the slick. The stream function ψ is introduced by

$$u=\frac{\partial\psi}{\partial y}, \quad v=-\frac{\partial\psi}{\partial x} \tag{2.1.26}$$

Following from the equation (2.1.21), the function ψ must satisfy

$$\frac{\partial^2\psi}{\partial y\partial t}+\frac{\partial\psi}{\partial y}\frac{\partial^2\psi}{\partial y\partial x}-\frac{\partial\psi}{\partial x}\frac{\partial^2\psi}{\partial y^2}=\nu\frac{\partial^3\psi}{\partial y^3} \tag{2.1.27}$$

Hoult [14] suggests that the similarity solution in this case takes the form

$$u=xt^{-1}F'(\beta) \tag{2.1.28}$$

where

$$\beta=\frac{y}{(\nu t)^{\frac{1}{2}}} \tag{2.1.29}$$

is the similarity variable. Buckmaster, in contrast, remarks that the boundary-layer thickness δ, in such a description, is independent of x, which must be incorrect in the vicinity of the leading edge.

As an improvement, Buckmaster [2] suggests the necessity of having two similarity variables

$$\gamma = \frac{x}{Ct^{\alpha}}, \quad \beta = \frac{y}{(\nu t)^{\frac{1}{2}}} \tag{2.1.30}$$

A similarity solution then is sought in the form

$$\psi = \nu^{\frac{1}{2}} x t^{-\frac{1}{2}} F(\gamma, \beta) \tag{2.1.31}$$

The function F then satisfies the equation

$$F_{\beta\beta\beta} + F_{\beta\beta}(\frac{1}{2}\beta + F) + F_{\beta} - F_{\beta}^2 = \gamma(F_{\beta}F_{\gamma\beta} - F_{\gamma}F_{\beta\beta} - \alpha F_{\gamma\beta}) \tag{2.1.32}$$

Also the boundary conditions for F can be derived. From condition (2.1.23), we immediately get

$$\begin{aligned} v(x,0;t) &= -\nu^{\frac{1}{2}} t^{-\frac{1}{2}} F(\gamma,0) - \nu^{\frac{1}{2}} x t^{-\frac{1}{2}} \tfrac{1}{Ct^{\alpha}} F_{\gamma}(\gamma,0) \\ &= -\nu^{\frac{1}{2}} t^{-\frac{1}{2}} F(\gamma,0) - \nu^{\frac{1}{2}} t^{-\frac{1}{2}} \gamma F_{\gamma}(\gamma,0) \\ &= 0 \\ &\Rightarrow F(\gamma,0) + \gamma F_{\gamma}(\gamma,0) = 0 \\ &\Rightarrow F(\gamma,0) = \frac{k}{\gamma}, \quad k \in \mathbb{R} \end{aligned}$$

Such a function $F(\gamma, 0)$ is defined at the center of the slick ($\gamma = 0$) only if $k = 0$. Thus

$$F(\gamma, 0) = 0 \tag{2.1.33}$$

At this moment, $q(x, t)$ is not known yet, but only a right choice of q will lead to a self-consistent solution. Hoult [14] shows that the oil continuity equation is identically satisfied, and h is finite at $x = 0$ if and only if

$$q = \alpha \frac{x}{t} \tag{2.1.34}$$

Therefore, (2.1.23) and (2.1.24) yield

$$\begin{aligned} &\frac{x}{t} F_{\beta}(\gamma,0) = \alpha \frac{x}{t}, \quad \lim_{\beta\to\infty} \frac{x}{t} F_{\beta}(\gamma,\beta) = 0 \\ &\Rightarrow F_{\beta}(\gamma,0) = \alpha, \quad \lim_{\beta\to\infty} F_{\beta}(\gamma,\beta) = 0 \end{aligned} \tag{2.1.35}$$

Now equation of function F(2.1.32) together with its boundary conditions is solvable. Buckmaster [2] suggests an effective way to solve this third order ODE is to expand $F(\gamma, \beta)$ as a series in γ, i.e.

$$F(\gamma,\beta) = F_0(\beta) + \sum_{n=1}^{\infty} C_n \gamma^{\omega_n} F_n(\beta) \tag{2.1.36}$$

where ω_n is a positive increasing sequence of real numbers. Then we can derive the equations satisfied by each F_n. As examples, for F_0 and F_1, the equations are

$$F_0''' + F_0''(\frac{1}{2}\beta + F_0) + F_0' - F_0'^2 = 0 \tag{2.1.37}$$

$$F_1''' + F_1''(\frac{1}{2}\beta + F_0) + F_1'(1 + \frac{3}{8}\omega_1 - 2F_0' - \omega_1 F_0') + F_1(1+\omega_1)F_0'' = 0 \tag{2.1.38}$$

The boundary conditions on F_n are then

$$F_n(0) = 0, \quad F_0'(0) = \alpha, \quad F_n'(0) = 0 (n \geq 1), \quad \lim_{\beta\to\infty} F_n'(\beta) = 0 \tag{2.1.39}$$

However, the above boundary conditions do not ensure a unique solution for F_n. Hoult [15] shows that two out of three solutions of (2.1.37) satisfy $F_0 = 0$ and $F_0'(\infty) = 0$. Buckmaster [2] also points out that the non-uniqueness of the solution can be isolated by considering the behavior for large β. By linearizing the solution at infinity, where F_n = constant, it can be seen that the solution for F_n' contains two independent terms,

$$\beta^{-2-\frac{3}{4}\omega_n}, \quad \beta^{1+\frac{3}{4}\omega_n} \exp[-\frac{1}{4}(\beta + 2F_n(\infty))^2] \tag{2.1.40}$$

Hence, any $F_n''(0)$ will give a solution that satisfies our boundary conditions. Therefore, we need specify the actual numbers for $F_n''(0)$ in order to solve the equation system.

Hoult [14] finds the value $F_0''(0) = 0.213$ through a one-dimensional experiment and he believes $F_0''(0)$ should have the same value in both one-dimensional and axisymmetric cases. While Buckmaster [2] suggests that we can determine $F_n''(0)$ without experimental results but based on the nature of the solution for F_n. Starting with F_0, the solution to (2.1.37) has been investigated numerically, for different choices of $F_0''(0)$ and $\alpha = \frac{3}{8}$. The graph of F_0', which contributes to the water velocity, are shown in Figure 2.4.

If $F_0''(0)$ is positive, there exist some points within the boundary layer at which the water velocity is larger than the slick velocity $q = \frac{3}{8}xt^{-1}$. This is unrealistic in the boundary-layer theory with the assumption that the free stream in the water is stable. We can therefore exclude such solutions.

If $F_0''(0) < -0.0124$, F_0' is negative in some region, which indicates an existence of reversed flows. Following Buckmaster [2], we argue that this is not physically reasonable.

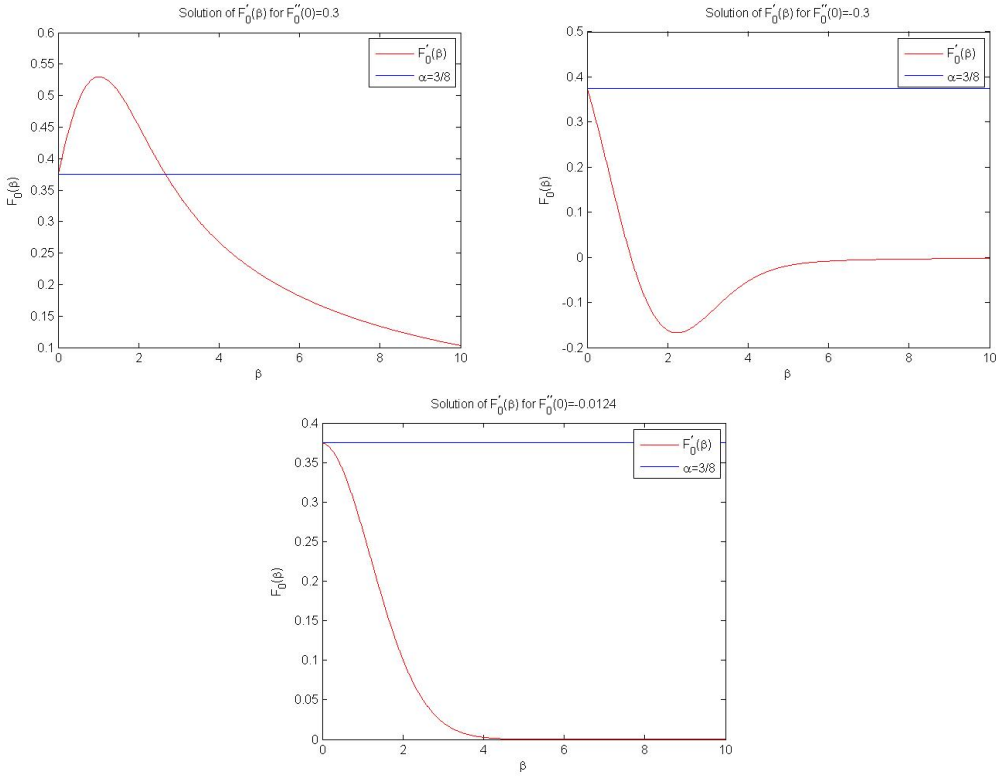

Figure 2.4: Solution of F_0' for different $F_0''(0)$

For $F_0''(0)$ in the interval $[-0.0124, 0]$, the water velocity u is monotone decreasing on β. More importantly, at the interval's left end point -0.0124, the water velocity F_0' approaches 0 exponentially at infinity, whereas for all other points its behaviour is algebraic. Such phenomenon has been justified in higher order boundary-layer theory by [1]. It is argued that the boundary-layer flow must approach the free-stream condition exponentially. Thus we can conclude that $F_0''(0) = -.0124$ is the appropriate boundary condition and with this F_0 can be solved uniquely.

Next let's turn to the equation (2.1.38) for F_1. Since its equation and boundary conditions are both homogeneous we may choose $F_1''(0) = 1$ without loss of generality. Again we want to force an exponential behaviour on F_1' at infinity, by appropriate choice of parameter ω_1. Actually, there are probably infinitely many possible ω_1 that will lead to an exponential behaved F_1'. Buckmaster [2] found the first two numbers that meet this requirement are

$$4.966, \quad 8.248$$

In principle, all ω_n and F_n can be determined in this manner. Unfortunately, this is still not enough to provide an unique solution to F because the coefficients C_n in the series expansion of F have not been specified. Buckmaster believes that this issue results from the fact that (2.1.36) is actually a 'downstream' expansion. Such non-uniqueness is typical of downstream expansions of steady boundary-layer flows because it fails to account for the initial conditions (upstream data). Therefore, he suggests it might be more useful to integrate from the leading edge of the slick [2].

2.1.3 Flows near the leading edge of the slick

To study the flows near the leading edge, we reset the coordinate frame at the right side edge of the slick so that the frame is moving with the edge of the slick, shown in Figure 2.5. Under this coordinate frame, the boundary-layer equation (2.1.21) is re-written as

$$\frac{\partial \tilde{u}}{\partial t} + \tilde{u}\frac{\partial \tilde{u}}{\partial \tilde{x}} + v\frac{\partial \tilde{u}}{\partial y} = \ddot{R} + \nu\frac{\partial^2 \tilde{u}}{\partial y^2} \tag{2.1.41}$$

$$\frac{\partial \tilde{u}}{\partial \tilde{x}} + \frac{\partial v}{\partial y} = 0 \tag{2.1.42}$$

where

$$\tilde{x} = R(t) - x, \quad \tilde{u} = \dot{R}(t) - u \tag{2.1.43}$$

Then the same 'no-slip' boundary conditions in this frame can be derived:

$$v(\tilde{x}, 0; t) = 0 \tag{2.1.44}$$

$$\lim_{y\to\infty} \tilde{u}(\tilde{x}, y; t) = \alpha C t^{\alpha-1}, \quad \lim_{\tilde{x}\to 0} \tilde{u}(\tilde{x}, 0; t) = 0 \tag{2.1.45}$$

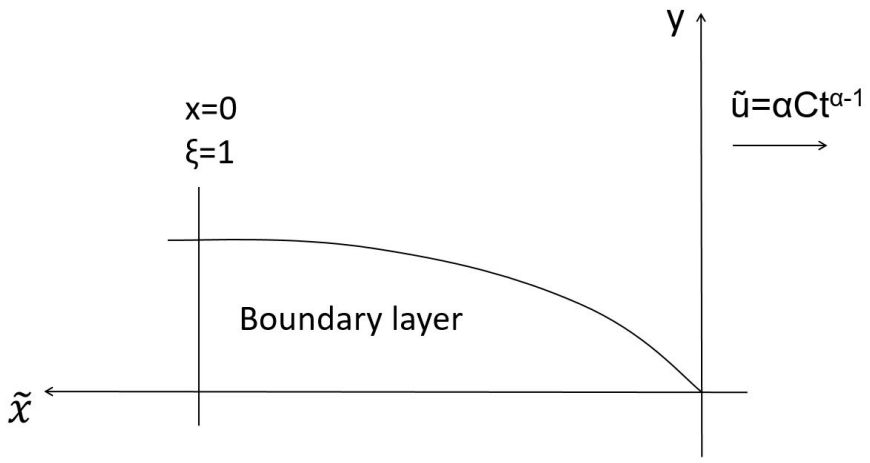

Figure 2.5: Boundary layer in leading edge frame

A new stream function is introduced by

$$\tilde{u} = \frac{\partial \tilde{\psi}}{\partial y}, \quad v = -\frac{\partial \tilde{\psi}}{\partial \tilde{x}} \tag{2.1.46}$$

The similarity solution then is sought in the form

$$\tilde{\psi} = (2\alpha C \nu \tilde{x} t^{\alpha-1})^{\frac{1}{2}} G(\xi, \eta) \tag{2.1.47}$$

where

$$\xi = \frac{\tilde{x}}{Ct^{\alpha}}, \quad \eta = y(\frac{\alpha C t^{\alpha-1}}{2\nu\tilde{x}})^{\frac{1}{2}} \tag{2.1.48}$$

are similarity variables. Then G must satisfy the equation

$$G_{\eta\eta\eta} + GG_{\eta\eta} = 2\xi(G_\eta G_{\eta\xi} - G_\xi G_{\eta\eta} - \xi G_{\eta\xi}) + 2\xi(\alpha-1)\alpha^{-1}(G_\eta + \frac{1}{2}\eta G_{\eta\eta} - 1) \tag{2.1.49}$$

And the corresponding boundary conditions are

$$G(\xi, 0) = 0, \quad \lim_{\eta\to\infty} G_\eta(\xi, \eta) = 1 \tag{2.1.50}$$

Now we expand G as a power series in ξ,

$$G(\xi, \eta) = \sum_{n=0}^{\infty} \xi^n G_n(\eta) \tag{2.1.51}$$

Note that in this expansion of G, there is no undetermined constant C_n.

Equation (2.1.49) then immediately leads to a sequence of equations satisfied by each G_n. The first two equations are

$$G_0''' + G_0 G_0''' = 0 \tag{2.1.52}$$

$$G_1''' + G_0 G_1''' - 2G_0' G_1' + 3G_0'' G_1 = \frac{10}{3} - \frac{10}{3}(G_0' + \frac{1}{2}\eta G_0'') \tag{2.1.53}$$

These equations will be solved with boundary conditions

$$G_n(0) = 0, \quad \lim_{\eta\to\infty} G_n'(\eta) = \delta_{n0}, \quad G_0'(0) = 0 \tag{2.1.54}$$

With the expansion of function G, the skin friction at the water-oil interface can be calculated

$$\frac{\partial \tilde{u}}{\partial y}(\tilde{x}, 0; t) = \frac{\partial^2 \psi}{\partial y^2}(\tilde{x}, 0; t) = (\alpha C t^{\alpha-1})^{\frac{3}{2}} (2\nu\tilde{x})^{-\frac{1}{2}} \sum_{n=0}^{\infty} \xi^n G_n''(0) \tag{2.1.55}$$

This allows us to integrate the oil momentum equation (2.1.18) to get the oil thickness h

$$\int h \frac{\partial h}{\partial x} dx = \frac{\nu}{g\Delta} \int \frac{\partial u}{\partial y}(x, 0; t) dx$$

$$\Rightarrow \frac{1}{2} h^2 = \frac{\nu}{g\Delta} (\alpha C t^{\alpha-1})^{\frac{3}{2}} (2\nu)^{-\frac{1}{2}} \sum_{n=0}^{\infty} \int \tilde{x}^{-\frac{1}{2}} \xi^n dx$$

$$\Rightarrow h^2 = (2\nu)^{\frac{1}{2}} (\alpha C)^{\frac{3}{2}} (g\Delta)^{-1} \tilde{x}^{\frac{1}{2}} t^{\frac{3}{2}(\alpha-1)} \sum_{n=0}^{\infty} \xi^n \frac{G_n''(0)}{n + \frac{1}{2}} \tag{2.1.56}$$

Now α can be determined by considering the volume of the slick. Suppose the oil slick has a constant volume V, then a half volume is obtained by integrating its thickness h from the leading edge to the center

$$\frac{1}{2} V = \int_0^R h d\tilde{x} = C t^{\alpha} \int_0^1 h(\xi) d\xi$$

$$\Rightarrow \frac{1}{2} V = C^2 \alpha^{\frac{3}{4}} (2\nu)^{\frac{1}{4}} (g\Delta)^{-\frac{1}{2}} t^{2\alpha - \frac{3}{4}} \int_0^1 \xi^{\frac{1}{4}} [\sum_{n=0}^{\infty} \frac{\xi^n G_n''(0)}{n + \frac{1}{2}}]^{\frac{1}{2}} d\xi \tag{2.1.57}$$

Assuming V is a constant, the right side of the above equation is only independent of time when $\alpha = \frac{3}{8}$.

In terms of the series expansion of function G, the velocity of the oil takes the form of

$$q = \dot{R}(t) - \frac{\partial \tilde{\psi}}{\partial y} = \alpha C t^{\alpha-1} - \alpha C t^{\alpha-1} \sum_{n=0}^{\infty} \xi^n G_n'(0) \tag{2.1.58}$$

In this moving frame, since

$$\frac{\partial h(x,t)}{\partial t} = \frac{\partial h(\tilde{x},t)}{\partial t} + \dot{R}\frac{\partial h(\tilde{x},t)}{\partial \tilde{x}}, \quad \frac{\partial h}{\partial x} = -\frac{\partial h}{\partial \tilde{x}}, \quad \frac{\partial q}{\partial x} = -\frac{\partial q}{\partial \tilde{x}}$$

The oil continuity equation in such frame can be written as

$$\begin{aligned} &\frac{\partial h}{\partial t} + \dot{R}\frac{\partial h}{\partial \tilde{x}} - q\frac{\partial h}{\partial \tilde{x}} - h\frac{\partial q}{\partial \tilde{x}} = 0 \\ \Leftrightarrow\ &\frac{\partial}{\partial t}(h^2) + \alpha C t^{\alpha-1}\frac{\partial}{\partial \tilde{x}}(h^2) - q\frac{\partial}{\partial \tilde{x}}(h^2) - 2h^2\frac{\partial q}{\partial \tilde{x}} = 0 \end{aligned} \tag{2.1.59}$$

Substituting the expressions of q (2.1.58) and h (2.1.56) into the above equation yields

$$\begin{aligned} &\sum_{n=0}^{\infty} \xi^{n+1} \frac{G_n''(0)}{n+\frac{1}{2}} [\frac{3(\alpha-1)}{2\alpha} - n] + \sum_{n=0}^{\infty} \xi^n G_n'(0) \sum_{n=0}^{\infty} \xi^n G_n''(0) \\ &+ 2\sum_{n=0}^{\infty} \frac{\xi^n G_n''(0)}{n+\frac{1}{2}} \sum_{n=0}^{\infty} \xi^n n G_n'(0) = 0 \end{aligned} \tag{2.1.60}$$

Then it can be verified that when $\alpha = \frac{3}{8}$, the solution of this infinite set of equations is

$$G_1'(0) = 1, \quad G_n'(0) = 0, n \geq 2 \tag{2.1.61}$$

Using this result for (2.1.58), the oil velocity q is then

$$q = \frac{3}{8}\frac{x}{t} \tag{2.1.62}$$

This is consistent with the initial assumption on q.

Subject to boundary conditions (2.1.61), G_n now are uniquely defined, and of more interest, the skin friction coefficients $G_n''(0)$ can be evaluated numerically. In principle, the thickness of the slick is now given by (2.1.56). Then the prefactor C can be determined by summing the series in (2.1.57). Solutions of the first few G_n' and G_n'' are shown in Figure 2.6.

And those actually are useful to the derivation are $G_n''(0)$, which are shown in Table 2.3. However, the values of $G_n''(0)$ are so large that the series in (2.1.57) cannot be easily summed, especially near the center of the slick ($\xi \sim 1$). Therefore, Buckmaster [2] solves for $G_{\eta\eta}(\xi, 0)$ for large ξ in a different way as follows.

Known that $q = \frac{3}{8}\frac{x}{t}$, the problem is to solve the equations

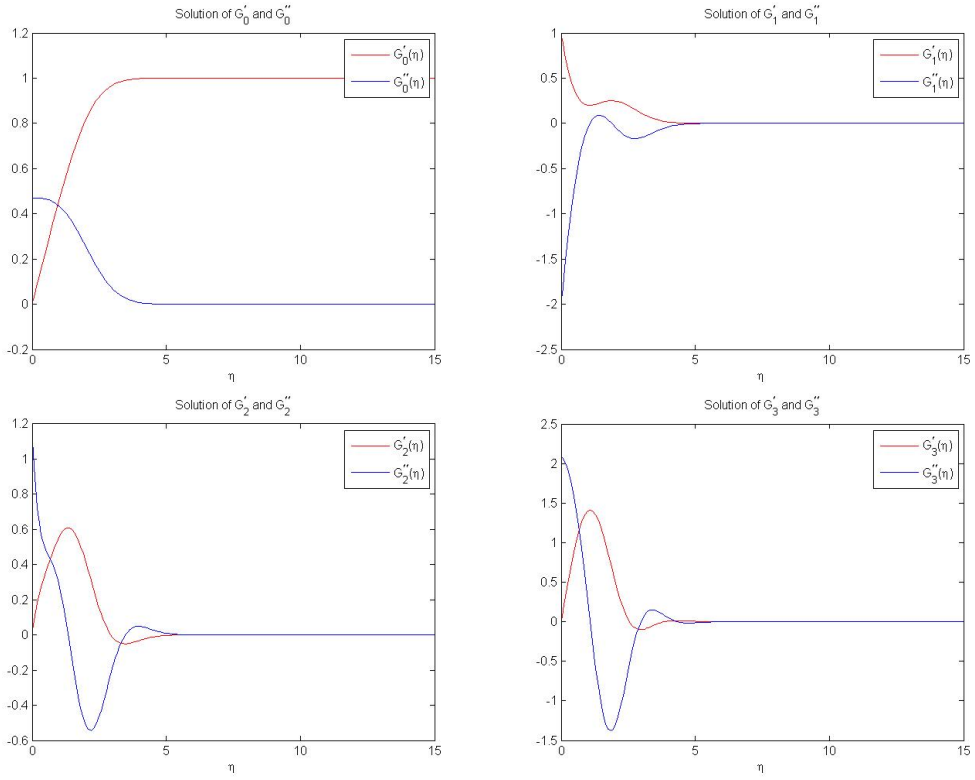

Figure 2.6: Solutions of G'_n and G''_n

n	0	1	2	3	4	5
$G''_n(0)$	0.469600	-2.002364	1.190562	2.077139	4.781272	8.714005

Table 2.3: Skin-friction coefficients

	$G_{\eta\eta}(\xi,0)$			$G_{\eta\eta}(\xi,0)$	
ξ	Terrill	series	ξ	Terrill	series
0	–	0.4696	0.275	0.084	0.095
0.025	–	0.420	0.30	0.072	0.093
0.05	–	0.373	0.325	0.062	0.103
0.075	–	0.327	0.35	0.055	–
0.10	–	0.284	0.40	0.045	–
0.125	0.244	0.244	0.50	0.036	–
0.15	0.207	0.207	0.60	0.028	–
0.175	0.173	0.173	0.70	0.021	–
0.20	0.144	0.145	0.80	0.015	–
0.225	0.119	0.121	0.90	0.008	–
0.25	0.099	0.104			

Table 2.4: Skin-friction coefficients

$$\frac{\partial \tilde{u}}{\partial t} + \tilde{u}\frac{\partial \tilde{u}}{\partial \tilde{x}} + v\frac{\partial \tilde{u}}{\partial y} = -\frac{5}{24}Ct^{-\frac{13}{8}} + \nu\frac{\partial^2 \tilde{u}}{\partial y^2} \tag{2.1.63}$$

$$\frac{\partial \tilde{u}}{\partial \tilde{x}} + \frac{\partial v}{\partial y} = 0 \tag{2.1.64}$$

subject to the boundary conditions

$$v(\tilde{(}x), 0; t) = 0, \quad \tilde{u}(\tilde{x}, 0; t) = \frac{3}{8}Ct^{-\frac{5}{8}}\xi \tag{2.1.65}$$

$$\lim_{y\to\infty} \tilde{u}(\tilde{x}, y; t) = \frac{3}{8}Ct^{-\frac{5}{8}} \tag{2.1.66}$$

The similarity solution of this system is numerically obtained from equation. Specifically, Buckmaster [2] starts using the series expansion that we just present above for small ξ, and then continues using essentially the method described by Terrill [25] to seek for $G_{\eta\eta}$. Eventually, the skin friction at the interface is of primary interest and was computed at intervals in ξ of 0.025 starting at $\xi = 0.1$, the point where the series expansion was abandoned. Table.3 shows Buckmaster's results with a comparison between the series expansion and Terrill's method.

Once the skin friction is known, the slick thickness may be found by (2.1.56). In Particular,

$$h \equiv \nu^{\frac{1}{4}}(g\Delta)^{-\frac{1}{2}}Ct^{-\frac{3}{8}}H(\xi) \tag{2.1.67}$$

The values of $H(\xi)$ are shown in Table.4.

ξ	$H(\xi)$	ξ	$H(\xi)$
0	0	0.15	0.308
0.002	0.117	0.20	0.319
0.004	0.138	0.30	0.329
0.006	0.153	0.40	0.334
0.008	0.164	0.50	0.337
0.01	0.173	0.60	0.339
0.02	0.205	0.70	0.340
0.03	0.225	0.80	0.341
0.05	0.252	0.90	0.342
0.075	0.274	1.0	0.342
0.10	0.289		

Table 2.5: Slick thickness coefficient

The last step of the calculation is integrating the thickness h to get the volume, through equation (2.1.57). This leads to a value of C so that the size of the slick following from this calculation is

$$R(t) = 1.76(g\Delta)^{\frac{1}{4}} V^{\frac{1}{2}} \nu^{-\frac{1}{8}} t^{\frac{3}{8}} \tag{2.1.68}$$

As a comparison, the experimental result by Hoult [14] shows that the coefficient best fits its data is 1.5. So the error in Buckmaster's result is approximately 17%. Buckmaster discusses the possible reasons for such an error and summaries that the boundary layer is perhaps turbulent, rather than laminar, as assumed here.

2.2 Modeling Crude Oil: Dimension Reduction and Data Assimilation

When modeling the spreading of crude oil on the water, a bulk model that are assumed in the previous sections are physically unrealistic, since crude oil is made of hundreds or even thousands of chemical components, each has different properties. Different components can react chemically with each other. They also dissolve into sea water or evaporate into the atmosphere at different rates. In practice, we do not have the remote sensing capabilities or the computational power needed to track each individual component. Consequently, the composition of the oil is uncertain, and it varies both temporally and spatially, which in turn leads to spreading rates that vary in both space and time. It is a significant mathematical challenge to track the evolution of hundreds of uncertain quantities for oil slick dynamics. A first step in this direction is a recent work by Venkatamarani, Venkataramani and Restrepo [27] on developing reduced, stochastic models for the high dimensional system describing the evaporation of multiple components in an oil spill. We will first review their work

on dimension reduction for systems with slow relaxation in this chapter and build on this work to develop statistical tools using data assimilation to simultaneously track the composition and the evolution of oil later.

2.2.1 The Linear Evaporation Process of Oil

As an example of systems with slow relaxation, let's consider the process of oil evaporation. Inspired from the equations for the evaporation of water, the evaporation of each compound in crude oil can be modeled as

$$E/C \approx KTS \tag{2.2.1}$$

where E is the evaporation rate, C is the concentration of the compound, K is the mass transfer rate, T is a coefficient that characterizes the transport of the vapor from the interface and S is a factor that depends on the saturation of the boundary layer by the evaporating fluid. It is natural to consider the quantity $\alpha = KTS$ as a constant, so called the evaporation rate constant, to lead

$$E = \alpha C \tag{2.2.2}$$

Thus, a generic dynamical system for the evaporation of crude oil, treated as composite of many individual chemical compounds can be written as

$$\partial_t c_i(t) = -\alpha_i c_i(t), \quad \alpha_i > 0, 1 \leq i \leq I, \tag{2.2.3}$$

where i is the index of compound, I is the total number of compounds, c_i is the concentration of the i^{th} compound and α_i is the evaporation rate constant of the i^{th} compound. For crude oil, $I \gg 1$ will be considered.

Since measuring the concentration c_i for each individual compound is practically impossible, it is reasonable to rather consider a single source of measurement $M(t)$. $M(t)$ can be viewed as a weighted average of the concentrations c_i, i.e.

$$M(t) = \sum_i \beta_i c_i(t) = \sum_i \beta_i c_i(0) e^{-\alpha_i t} \tag{2.2.4}$$

By interpolating the values of α_i and β_i, one can replace the discrete index i with a continuous variable ω

$$\alpha_i = \alpha_{min}(1-\omega) + \alpha_{max}\omega \tag{2.2.5}$$

Let $i(\omega)$ denote a monotonic interpolation of the inverse of $\omega(i)$ and $\rho(\omega, t)$ the smooth interpolation of the function

$$\rho(\omega(i), t) = e^{\alpha_{min} t} \beta_i c_i \frac{\alpha_{max} - \alpha_{min}}{\alpha_{i+1} - \alpha_i} \tag{2.2.6}$$

It then yeilds that

$$M(t) = e^{-\alpha_{min}t} \sum_i \rho(\omega(i), t)[\omega(i+1) - \omega(i)] \tag{2.2.7}$$

Relying on the differential equations for c_i, the equation for $\rho(\omega, t)$ can be derived

$$\partial_t \rho(\omega, t) = -(\alpha_{max} - \alpha_{min})\omega\rho(\omega, t) \tag{2.2.8}$$

With a rescale on t and $\alpha_{min} = 0$, taking the continuum limits of equations (2.2.7) and (2.2.8) gives

$$\begin{aligned} \partial_t \rho(\omega, t) &= -\omega\rho(\omega, t) \\ M(t) &= \int_0^1 \rho(\omega, t) d\omega \end{aligned} \tag{2.2.9}$$

Model (2.2.9) are the continuum limit version of dynamical system (2.2.3). These two equations together with an initial condition $\rho(\omega, 0)$ define a linear evaporation process. The initial measure $\rho(\omega, 0)$ reflects the uncertainties in the initial composition of the oil and therefore can be viewed as a random state. In particular, the statistics of $\rho(\omega, t)$ should be inferred from the statistics of the concentrations $c_i(0)$ of each distinct compound in the oil. Both model (2.2.9) and model (2.2.3) are high dimensional system since a description on the microscopic structure is required to solve the system. We will review a dimension reduction procedure for this linear evaporation process in the following section.

2.2.2 The Mori-Zwanzig Decomposition of The Linear Evaporation

The derivation of the reduced model relies on the discrete-time Mori-Zwanzig projection. Suppose we take $\mathcal{H} = L^2([0, 1])$, the space of square integrable functions on [0,1]. We will use ket-vectors to represent states in $\mathcal{H}$ and use bra-vectors to represent observables.

Let's consider a discrete dynamical system for the linear evaporation process. $|\rho_n\rangle$ is the state of the microscopic structure of the oil, $M_n = \int \rho_n d\omega = \langle 1|\rho_n\rangle$ can be viewed as the weighted average of species concentration and is our single observed quantity. Suppose we have $|\rho_n\rangle = \Lambda|\rho_n\rangle$, where $\Lambda : \mathcal{H} \to \mathcal{H}$ is a linear operator on the space $\mathcal{H}$. Then we can decompose $|\rho_n\rangle$ as

$$|\rho_n\rangle = |\xi_n\rangle + |\eta_n\rangle \tag{2.2.10}$$

with

$$|\xi_n\rangle = P|\rho_n\rangle \quad |\eta_n\rangle = Q|\rho_n\rangle$$

where $P = |1\rangle\langle 1|$ is an orthogonal projection on $\mathcal{H}$ and $Q = I - P$ is the complementary projection. Explicitly, $|\xi_n\rangle = |1\rangle\langle 1|\rho_n\rangle = M_n|1\rangle$ and $M_n = \langle 1|\xi_n\rangle$. By induction, it is easy to show that

$$\begin{aligned}
|\rho_n\rangle &= |\xi_n\rangle + |\eta_n\rangle = |\xi_n\rangle + Q\Lambda(|\xi_{n-1}\rangle + |\eta_{n-1}\rangle) \\
&= |\xi_n\rangle + Q\Lambda|\xi_{n-1}\rangle + (Q\Lambda)^2(|\xi_{n-2}\rangle + |\eta_{n-2}\rangle) \\
&\vdots \\
&= \xi_n + \sum_{k=1}^{n}(Q\Lambda)^k|\xi_{n-k}\rangle + (Q\Lambda)^n Q|\rho_0\rangle
\end{aligned}$$

Therefore,

$$\begin{aligned}
M_n &= \langle 1|\xi_n\rangle = \langle 1|P|\rho_n\rangle = \langle 1|P\Lambda|\rho_{n-1}\rangle \\
&= \langle 1|P\Lambda|\xi_{n-1}\rangle + \sum_{k=2}^{n}\langle 1|P\Lambda(Q\Lambda)^{k-1}|\xi_{n-k}\rangle + \langle 1|P\Lambda(Q\Lambda)^{n-1}Q|\rho_0\rangle \\
&= \sum_{k=1}^{n}\langle 1|(\Lambda Q)^{k-1}\Lambda|1\rangle M_{n-k} + \langle 1|(\Lambda Q)^n|\rho_0\rangle
\end{aligned}$$

gives the Mori-Zwanzig decomposition of the linear evaporation process:

$$M_n = \sum_{k=1}^{n} h_k M_{n-k} + \beta_n, \tag{2.2.11}$$

where $h_k = \langle 1|(\Lambda Q)^{k-1}\Lambda|1\rangle$ and $\beta_n = \langle 1|(\Lambda Q)^n|\rho_0\rangle$ is the noise term that depends on the initial state $|\rho_0\rangle$. For the trivial case, where $|\rho_0\rangle = c|1\rangle$ for some constant c, one can explicitly solve the model (2.2.9) to have

$$M_n = c\int_0^1 e^{-\omega n\tau}d\omega = c\frac{1-e^{-n\tau}}{n\tau}, \quad n \geq 1 \tag{2.2.12}$$

Therefore, the corresponding memory kernel h_k for this case can be determined analytically by solving the equation

$$\frac{1-e^{-n\tau}}{n\tau} = \sum_{k=1}^{n} h_k \frac{1-e^{-(n-k)\tau}}{(n-k)\tau}, \quad n \geq 1 \tag{2.2.13}$$

Let the $\mathcal{Z}$-transform of M be $\hat{M}(z) = \sum_{n=0}^{\infty} M_n z^{-n}$ and $\hat{H}(z) = \sum_{n=0}^{\infty} h_n z^{-n}$. Then we multiply both sides of the above equation by z^{-n} and sum it over $n \geq 1$ to yield

$$\frac{1-e^{-n\tau}}{n\tau}z^{-n} = \sum_{k=1}^{n} h_k z^{-n} \frac{1-e^{-(n-k)\tau}}{(n-k)\tau}$$

$$\Rightarrow \frac{1}{M_0}\sum_{n=1}^{\infty} M_n z^{-n} = \frac{1}{M_0}\sum_{n=1}^{\infty}\sum_{k=1}^{n} h_k z^{-n} M_{n-k}$$

$$\Rightarrow \hat{M(z)} - M_0 = \hat{M(z)}\hat{H(z)} \tag{2.2.14}$$

So that

$$\hat{H(z)} = 1 - \frac{M_0}{\hat{M(z)}} \tag{2.2.15}$$

On the other hand, since M_n decreases over time, the series of $\hat{M}$ converges for all $|z| > 1$ so that the sum is computable.

$$\hat{M}(z) = M_0 \sum_{n=0}^{\infty} \int_0^1 e^{-\omega n\tau} z^{-n} d\omega = M_0 \int_0^1 \frac{ze^{\omega\tau}}{ze^{\omega\tau}-1} d\omega = \frac{M_0}{\tau}\ln(\frac{ze^{\tau}-1}{z-1}) \tag{2.2.16}$$

Substitution of this into equation (2.2.15) yields

$$\hat{H(z)} = 1 - \frac{\tau}{\ln(e^{\tau}z-1) - \ln(z-1)} \tag{2.2.17}$$

Expanding the resulting expression of $\hat{H(z)}$ about $z = \infty$ gives

$$\hat{H(z)} = \frac{1-e^{-\tau}}{\tau}z^{-1} + \frac{(1-e^{-\tau})((\tau-2)+(\tau+2)e^{-\tau}}{2\tau^2}z^{-2} + \cdots \tag{2.2.18}$$

So that the memory kernel h_k are given by

$$h_1 = \frac{1-e^{-\tau}}{\tau}, \quad h_2 = \frac{(1-e^{-\tau})((\tau-2)+(\tau+2)e^{-\tau}}{2\tau^2}, \quad \cdots \tag{2.2.19}$$

The asymptotic behavior of h_k is particularly interested. Flajolet and Odlyzko [10] have shown that

$$h_k \sim \frac{1}{k\ln^2 k}, \quad k \to \infty \tag{2.2.20}$$

using the transfer operator methods. It indicates that h_k decays algebraically and thus has a fat tail. One should expect such a slow decay since it reflects the slow relaxation in $\rho(\omega, t) = \rho_0(\omega)e^{-\omega t}$ for oil compounds with small ω.

For a general problem, in which the initial state $\rho_0(\omega)$ is random with uncertainty, the purpose of the following section is to estimate the single observable quantity M_n,

given the sequence of noisy measurements $_k = \langle 1|\rho_k\rangle + \gamma_k\sigma$ at the discrete time in the past, where γ_k are uncorrelated normal variables. The optimal estimator of M_n is given in terms of conditional expectation

$$\bar{M}_n = E[M_n|_{n-1,n-2}\,,\cdots,_0\,] \tag{2.2.21}$$

Evaluations on this expectation will reveal practical methods to predict the states of oil during its evaporation. In particular, one would like to seek for a function F_n such that

$$F_n(_{n-1,n-2}\,,\cdots,_0\,) \approx E[M_n|_{n-1,n-2}\,,\cdots,_0\,] \tag{2.2.22}$$

Next, we will present several possible estimators that are derived already in the paper [27].

2.2.3 Mori-Zwanzig Linear Autonomous Estimators

Based on the Mori-Zwanzig decomposition (2.2.11), if one replace β_n by a Gaussian process θ_n, which has the same statistical features with β_n, i.e.

$$E[\theta_n] = E[\beta_n] = 0, \quad E[\theta_n^T\theta_m] = E[\beta_n^T\beta_m], \quad m,n \geq 0 \tag{2.2.23}$$

then it gives a reduced stochastic model of the linear evaporation process (2.2.9),

$$M_n = \sum_{k=1}^{n} h_k M_{n-k} + \theta_n \tag{2.2.24}$$

An estimator that directly comes from this reduced model is

$$\bar{M}_n = \sum_{k=1}^{n} h_k \tilde{M}_{n-k} \tag{2.2.25}$$

We will refer this estimator as the MZ estimator. The MZ estimator is autonomous since it does not depend on n.

However, all history states $M_k, k = 0, 1, \cdots, n-1$ are required to estimate the current state. Since the memory kernel h_k decays slowly, reasonable estimate will not be guaranteed with a naive truncation on the sum at a fixed number of terms. As an illustration of the effect of the truncated sum, we will compare the estimator result from truncating the MZ decomposition at $L = 6$ with the estimator that tracks the entire history in section. The choice of the number of truncated terms $L = 6$ has no analytic reason other than presenting an example. In particular, because the quantity $h_k M_{n-k}$ have positive means and their sum over $n - L \leq k < n$ for a fixed L is $O(n^{-1})$, thus truncating the sum (2.2.25) will cause the estimator to be biased at $O(n^{-1})$. One can still try to reduce the bias by renormalizing the weights, i.e.

$$h_k^{'} = \frac{h_k}{\sum_{k=1}^{L} h_k}, \quad \bar{M}_n = \sum_{k=1}^{L} h_k^{'} \bar{M}_{n-k} \tag{2.2.26}$$

so that $\sum_{k=1}^{L} h_k^{'} = \sum_{k=1}^{\infty} h_k = 1$. The renormalized estimator has a bias $O(n^{-2})$. We will refer this estimator as the truncated FIR (finite impulse response) estimator.

An alternative way to truncate the MZ decomposition is to approximate the $\mathcal{Z}$-transform $\hat{H}(z)$ in by a rational function in z^{-1}, i.e.

$$\hat{H}(z) \approx \frac{p(z^{-1})}{q(z^{-1})}$$

where p and q are polynomials of degrees no more than L. Follows from (2.2.15), a approximated $\hat{M}(z)$ is given by

$$\hat{M}(z) \approx \frac{M_0}{1 - \frac{p(z^{-1})}{q(z^{-1})}} = M_0 \frac{q(z^{-1})}{q(z^{-1}) - p(z^{-1})} = M_0 \frac{q(z^{-1})}{b(z^{-1})}$$

One can also normalize q and b by requiring that $q(0) = 1$ and $p(0) = 0$. Suppose $b(z^{-1}) = 1 + b_1 z^{-1} + b_2 z^{-2} + \cdots + b_L z^{-L}$ and $q(z^{-1}) = 1 + q_1 z^{-1} + q_2 z^{-2} + \cdots + q_L z^{-L}$, we have

$$\begin{aligned}
&(1 + b_1 z^{-1} + b_2 z^{-2} + \cdots + b_L z^{-L}) \hat{M}(z) = M_0 (1 + q_1 z^{-1} + q_2 z^{-2} + \cdots + q_L z^{-L}) \\
&\Rightarrow (M_n + b_1 M_{n-1} + b_2 M_{n-2} + \cdots + b_L M_{n-L}) z^{-n} = M_0 q_n z^{-n} \\
&\Rightarrow M_n = M_0 q_n - \sum_{k=1}^{L} b_k M_{n-k}
\end{aligned}$$

This suggests an estimator of M_n

$$\bar{M}_n = M_0 q_n - \sum_{k=1}^{L} b_k \tilde{M}_{n-k} \tag{2.2.27}$$

2.2.4 Nonlinear Harmonic Filters

One motivation of seeking for nonlinear estimators is that the linear evaporation process has slow relaxation and the observed quantity M_n decays as $\frac{1}{n}$ roughly. This inspires us to estimate $\frac{1}{M_n}$ by looking for the estimator such that

$$\frac{1}{\bar{M}_n} = \sum_{k=1}^{n} \frac{v_k}{\tilde{M}_{n-k}} \tag{2.2.28}$$

Again, one can still expect to solve for the weights v_k from the trivial process (2.2.12), similar to the linear estimator part. In particularly, assuming $|\rho_0\rangle = |1\rangle$, we have

$$\frac{1}{M_n} = \frac{n\tau}{M_0(1-e^{-n\tau})} = \frac{n\tau}{M_0} + \frac{n\tau e^{-n\tau}}{M_0} + \frac{n\tau e^{-2n\tau}}{M_0} + \cdots, \quad n \geq 1 \tag{2.2.29}$$

The $\mathcal{Z}$-transform of $\frac{1}{M_n}$ is

$$T(z) = \sum_{n=0}^{\infty} \frac{1}{M_n} z^{-n} = \frac{1}{M_0}[1 + \frac{z^{-1}\tau}{(1-z^{-1})^2} + \sum_{j=1}^{\infty} \frac{z^{-1}\tau e^{-j\tau}}{(1-e^{-j\tau}z^{-1})^2}] \tag{2.2.30}$$

We want to solve for v_k through its $\mathcal{Z}$-transform by solving

$$S(z) = \sum_{k=0}^{\infty} v_k z^{-k} = z[1 - \frac{1}{M_0 T(z)}] \tag{2.2.31}$$

However, since the zeros of $T(z)$ are unknown so that the poles of $S(z)$ are unknown, we will not know the asymptotic behavior of v_k from this equation. Instead, one can use a rational approximation of $T(z)$ to help generate finite lag estimator for M_n^{-1}.

Since the series expansion of $\frac{1}{M_n}$ (2.2.29) converges exponentially, one can truncate the sum at order $e^{-mn\tau}$ to have

$$M_0 T(z) \approx 1 + \frac{z^{-1}\tau}{(1-z^{-1})^2} + \frac{z^{-1}\tau e^{-\tau}}{(1-e^{-\tau z^{-1}})^2} + \cdots + \frac{z^{-1}\tau e^{-m\tau}}{(1-e^{-m\tau}z^{-1})^2} \tag{2.2.32}$$

This gives a rational approximation of $T(z) = M_0^{-1} \frac{q(z^{-1})}{b(z)^{-1}}$ that one can use to develop a linear estimator for M_n^{-1}. An example calculation for $m = 1$ is the following.

$$\begin{aligned} T(z) &\approx \frac{1}{M_0}[1 + \frac{z^{-1}\tau}{(1-z^{-1})^2} + \frac{z^{-1}\tau e^{-\tau}}{(1-e^{-\tau z^{-1}})^2}] \\ &= \frac{1}{M_0} \frac{(1-z^{-1})^2(1-e^{-\tau}z^{-1})^2 + z^{-1}\tau[(1-z^{-1})^2 + (1-e^{-\tau}z^{-1})^2]}{(1-z^{-1})^2(1-e^{-\tau}z^{-1})^2} \end{aligned}$$

So the polynomials b and q are defined by

$$b(z^{-1}) = (1-z^{-1})^2(1-e^{-\tau}z^{-1})^2 \tag{2.2.33}$$

$$q(z^{-1}) = (1-z^{-1})^2(1-e^{-\tau}z^{-1})^2 + z^{-1}\tau[(1-z^{-1})^2 + (1-e^{-\tau}z^{-1})^2] \tag{2.2.34}$$

Then by a similar argument as in the linear estimator part, one can have the estimator for M_n^{-1},

$$\bar{M}_n^{-1} = \tilde{M}_0^{-1} q_n - \sum_{k=1}^{n} b_k \tilde{M}_{n-k}^{-1} \tag{2.2.35}$$

Since the polynomial b and q have degree $2m+2$ in general, corresponding to the $m+1$ quadratic factors from the poles of order 2 in the rational approximation of $T(z)$, the sum in (2.2.35) has at most $2m+2$ non-zero terms. We will refer the estimator (2.2.35) as a nonlinear harmonic estimator.

2.2.5 Empirical Estimators

In the previous two sections, the coefficients of the linear autonomous estimator and the harmonic estimators are derived from a particular sequence of M_n corresponding to the initial condition $|\rho_0\rangle = M_0|1\rangle$. Alternatively, another common approach to determining the parametric coefficients is comparing the reduced model with the data. In particular, one can use the linear estimator and the harmonic estimator as an ansatzes and infer the coefficients from random realizations of the time series M_n with initial conditions $|\rho_0\rangle$ sampled from an appropriate distribution.

We will use equation (2.2.11) as a state space model for M_n, where β_n is now considered as non-stationary random process. As a approximation, it is also assumed that the following model gives a stochastic parameterization of M_n.

$$\bar{M}_n = M_0 q_n + \sum_{k=1}^{min(n,L)} h_k M_{n-k} + \sigma(M_{n-1}, M_{n-2}, \ldots, M_0)\theta_n \tag{2.2.36}$$

where q_k, h_k are renormalized weights that are zero for $n > L$, and θ_n are i.i.d. normal variables.

2.2.6 Asymptotic Estimators

For the numerical discretization of the linear evaporation process, let's take

$$\rho_0(\omega) = \sum_{i=1}^{I} \frac{1}{I} \gamma_i \delta(\omega - (\frac{i}{I} - \frac{1}{2I})) \tag{2.2.37}$$

where I is the total number of discetized intervals of $[0,1]$, γ_i are non-negative i.i.d. random variables with mean μ_γ, variance σ_γ^2, and δ is the Dirac delta function. For continuous functions ϕ, ψ on $[0,1]$, one can show that

$$\mathrm{E}[\int_0^1 \rho_0(\omega)\psi(\omega)d\omega] = \mu_\gamma \sum_{i=1}^{I} \frac{1}{I} \phi(\frac{i}{I} - \frac{1}{2I}) \approx \mu_\gamma \int_0^1 \phi(x)dx \tag{2.2.38}$$

and

$$\begin{aligned}
&\mathrm{E}[\int_0^1 \int_0^1 \phi(\omega)\psi(\omega^{'})\rho_0(\omega)\rho_0(\omega^{'})d\omega d\omega^{'}] \\
&= (\mu_\gamma \sum_{i=1}^{I} \frac{1}{I}\phi(\frac{i}{I} - \frac{1}{2I}))^2 + \sigma_\gamma^2 \sum_{i=1}^{I} \frac{1}{I}\phi(\frac{i}{I} - \frac{1}{2I})\psi(\frac{i}{I} - \frac{1}{2I}) \\
&\approx \mu_\gamma^2 \int\int \phi(\omega)\psi(\omega^{'})d\omega d\omega^{'} + \frac{\sigma_\gamma^2}{I}\int \phi(\omega)\psi(\omega^{'})d\omega d\omega^{'}
\end{aligned} \tag{2.2.39}$$

Therefore, for the linear evaporation process $M_n = \langle 1|\Lambda^n|\rho_0\rangle$, assuming that the random initial condition $|\rho_0\rangle$ is normalized such that $M_0 = 1$, we have

$$\mathrm{E}[M_n] = \mathrm{E}[\langle 1|\Lambda^n|\rho_0\rangle] = \langle 1|\Lambda^n|1\rangle = \frac{1 - e^{-n\tau}}{n\tau}$$

and

$$\mathrm{E}[M_n M_j] = \langle 1|\Lambda^n|\mathrm{E}[|\rho_0\rangle\langle\rho_0|]\Lambda^j|1\rangle = \mathrm{E}[M_n]\mathrm{E}[M_j] + \sigma^2\langle 1|\Lambda^{n+j}|1\rangle$$

This suggests

$$\mathrm{Cov}(M_n, M_j) = \sigma^2\langle 1|\Lambda^{n+j}|1\rangle = \sigma^2\frac{1 - e^{(n+j)\tau}}{(n+j)\tau} \tag{2.2.40}$$

We are looking for an optimal estimator of the form

$$M_n = q_n M_0 + h_1^n M_{n-1} + h_2^n M_{n-2} + \cdots + h_L^n M_{n-L} + \theta_n$$

Note that the coefficients in the optimal estimator are allowed to be time dependent so that the estimator is not autonomous. Because of the orthogonality of the noise θ_n to M_n, one can have the Yule-Walker equations

$$\mathrm{E}[M_n M_{n-k}] = q_n \mathrm{E}[M_{n-k}] + \sum_{j=1}^{L} h_j^n \mathrm{E}[M_{n-j}M_{n-k}] \tag{2.2.41}$$

$$\mathrm{E}[M_n] = q_n + \sum_{j=1}^{L} h_j^n \mathrm{E}[M_{n-j}] \tag{2.2.42}$$

$$(2.2.41) - (2.2.42) \times \mathrm{E}[M_{n-k}] \Rightarrow \mathrm{Cov}(M_n, M_{n-k}) = \sum_{j=1}^{L} h_j^n \mathrm{Cov}(M_{n-j}, M_{n-k})$$

$$\Rightarrow \frac{1 - e^{-(2n-k)\tau}}{(2n-k)\tau} = \sum_{j=1}^{L} h_j^n \frac{1 - e^{-(2n-k-j)\tau}}{(2n-k-j)\tau}, \quad k = 1, 2, , \ldots, L \tag{2.2.43}$$

For a long period of time, one can ignore the exponential terms to get a linear system

$$\underbrace{\begin{bmatrix} \frac{1}{2n-1} \\ \frac{1}{2n-2} \\ \vdots \\ \frac{1}{2n-L} \end{bmatrix}}_{v} = \underbrace{\begin{bmatrix} \frac{1}{2n-2} & \frac{1}{2n-3} & \cdots & \frac{1}{2n-L-1} \\ \frac{1}{2n-3} & \frac{1}{2n-4} & \cdots & \frac{1}{2n-L-2} \\ \vdots & \vdots & \ddots & \vdots \\ \frac{1}{2n-L-1} & \frac{1}{2n-L-2} & \cdots & \frac{1}{2n-2L} \end{bmatrix}}_{A} \underbrace{\begin{bmatrix} h_1^n \\ h_2^n \\ \vdots \\ h_L^n \end{bmatrix}}_{h} \tag{2.2.44}$$

The difficulty of solving this system is that the coefficients matrix A is ill conditioned. We can see this through expanding the matrix as a series in n:

$$A = \frac{1}{2n}\begin{bmatrix} 1 & 1 & \cdots & 1 \\ 1 & 1 & \cdots & 1 \\ \vdots & \vdots & \ddots & \vdots \\ 1 & 1 & \cdots & 1 \end{bmatrix} + \frac{1}{4n^2}\begin{bmatrix} 2 & 3 & \cdots & L+1 \\ 3 & 4 & \cdots & L+2 \\ \vdots & \vdots & \ddots & \vdots \\ L+1 & L+2 & \cdots & 2L \end{bmatrix} + \cdots$$

The first $L-1$ matrices in the expansion of A are all singular and their row null spaces are nested. The determinant of A is so close to zero that it is not clear that there is a solution for h^n where the leading order stays $O(1)$ rather than diverging. However, we can still solve this system based on its special structure. According to [22], A is a Cauchy matrix whose entries are of the form $A_{ij} = 1/(x_i - y_j)$, with $x_i = 2n - i$ and $y_j = j$. Its determinant is given by

$$\det(A) = \frac{\prod_{i>j}(x_i - x_j)(y_j - y_i)}{\prod_i \prod_j (x_i - y_j)}$$

Let's create another matrix $\hat{A}_m$ by replacing the m^{th} column of A with the vector $v_i = \frac{1}{2n-i}$. The resulting matrix $\hat{A}_m$ is still a Cauchy matrix with the choice $x_i = 2n-i$ and

$$\hat{y}_i = \begin{cases} y_j, & j \neq m \\ 0, & j = m \end{cases}$$

Then by Cramer's rule, the unique solution of this system is computed as h_j^n:

$$\begin{aligned} h_j^n = \frac{\det(\hat{A}_j)}{\det(A)} &= \prod_{i \neq j}^{L} \frac{i}{i-j} \prod_{i=1}^{L} \frac{2n-i-j}{2n-i} \\ &= (-1)^{j-1}\binom{L}{j} + (-1)^j \frac{L^2}{2n}\binom{L-1}{j-1} + O(n^{-2}) \end{aligned} \tag{2.2.45}$$

As an example, if we take $L = 6$, the coefficients are

$$h_1^n = 6 - \frac{36}{2n-1}$$

$$h_2^n = -15 + \frac{630}{2n-1} - \frac{225}{n-1}$$

$$h_3^n = 20 - \frac{3360}{2n-1} + \frac{2100}{n-1} - \frac{1200}{2n-3}$$

Asymptotically, the estimator coefficients converges as $n \to \infty$,

$$\lim_{n\to\infty} h_j^n = (-1)^{j-1}\binom{L}{j} \tag{2.2.46}$$

We will refer the estimator

$$\bar{M}_n = \sum_{j=1}^{L} h_j^n M_{n-j} \tag{2.2.47}$$

together with coefficients given by (2.2.45) as the asymptotic estimator.

2.2.7 Performance Of The Estimators

In this section, we will compare the estimators that were mentioned in the last section and their performances on predicting the linear evaporation process.

For simplicity, the data that is used for the estimation and comparison is generated through a synthetic experiment. In particular, the data is generated by the following Algorithm.

Algorithm 1 Generate synthetic data for M_n

$I = 1000$, $\Delta = 1/I$
Draw u_i from $\mathcal{U}(0,1)$, $i = 1, 2, \cdots, I$
$\rho_0(i) = u_i/(\Delta \sum_{i=1}^{I} u_i)$
$\omega(i) = (i - \frac{1}{2})\Delta$, $i = 1, 2, \cdots, I$
$\tau = \ln(3/2)$
for n=1:N **do**
  $\rho_n(i) = \rho_0(i)(2/3)^{n\omega(i)}$
  $M_n = \sum_{i=1}^{I} \rho_n(i)\Delta$
end for

For each estimator, the one step error defined as $|\bar{M}_n - M_n|$ is used to evaluate its performance on prediction. The quantity $\bar{M}_n$ is estimated oil concentration using

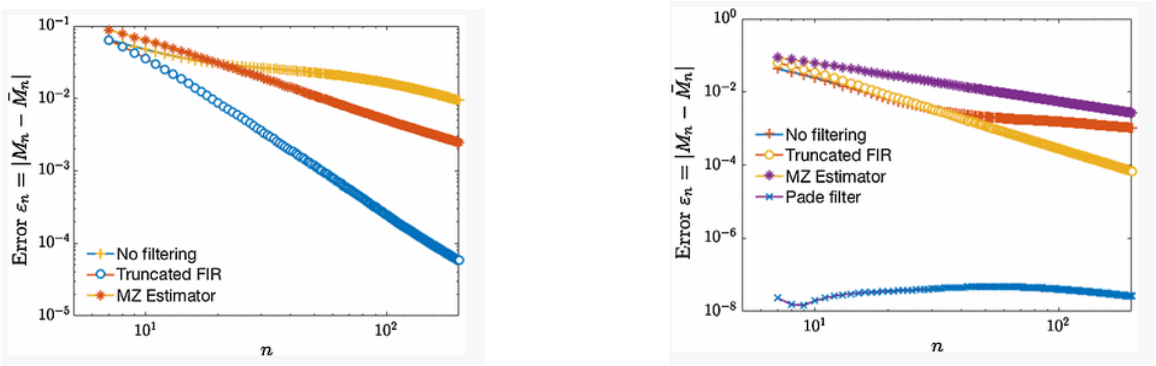

(a) (b)

Figure 2.7: Performance of MZ Estimators. Figure captured from [27]

the information available at time $n-1$, while M_n is the 'truth' given by the synthetic data.

In Figure 2.7, the performances of MZ estimators with different truncation are compared by its averaged one step error over 100 realizations. The no filtering process is essentially the trivial process (2.2.9) with no 'noise' in the initial condition. The MZ estimator is the estimator (2.2.25) derived from the Mori-Zwanzig decomposition of the linear evaporation process, while predicting using all history states. The Truncated FIR estimator is the MZ estimator truncated naively at a finite terms $L = 6$. From Figure 2.7a, we see that the Truncated FIR estimator performs surprisingly better than the MZ estimator even though we know that the estimator's memory kernel decays slowly.

In Figure 2.7b, the Pade estimator is derived from approximating $H(z)$ about $z = \infty$ using the Pade approximation to obtain 6^{th} order polynomials p and q, which give arise to a 6 tap estimator of the form (2.2.25). Once again, the Pade estimator, which is intended to approximate the MZ estimator using fewer history states, performs even better than the MZ estimator.

Figure 2.8 is showing a comparison between the Nonlinear Harmonic estimators with different truncation and the Pade estimator. The three Harmonic estimators correspond to truncating the series expansion of M_n^{-1} (61) at order $e^{-mn\tau}$, where $m = 0, 1$ and 2. We see from the figure that the Pade estimator performs better than the Nonlinear Harmonic estimators at predicting the first few time steps up to 50. However, the Nonlinear Harmonic estimators have comparable or even better predictions on a longer period of time.

In the next, Figure 2.9 presents the performances of the Empirical estimator and the Empirical Harmonic estimator. The one step errors are computed for each estimator on a single realization and are averaged over 100 random realizations that are not in the training set as well. As comparison, a Linear Oracle, which is an estimator

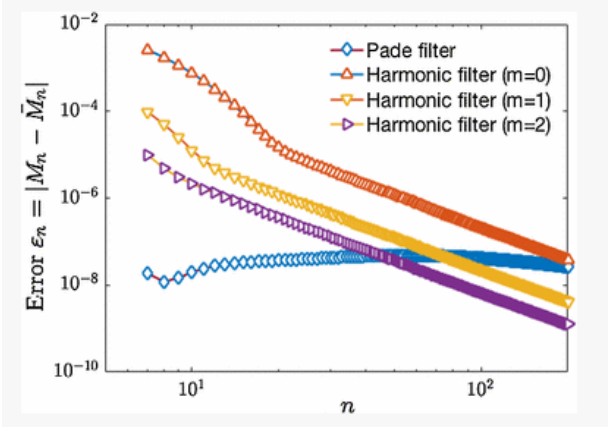

Figure 2.8: Performances of Harmonic estimator. Captured from [27]

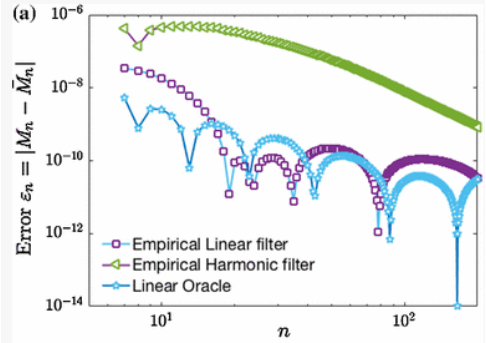

(a) Empirical estimator errors on a single realization

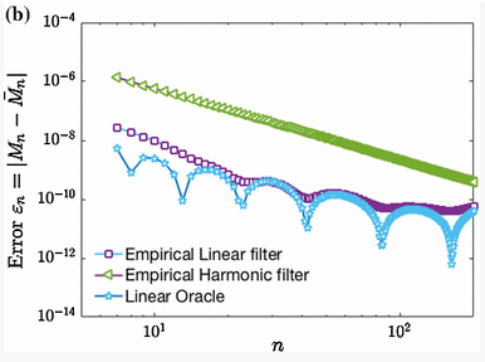

(b) Empirical estimator errors averaged on 100 realizations

Figure 2.9: Performance of Empirical Estimators. Captured from [27]

resulting from minimizing the sum of the residual squares over all sub-sequences of consecutive values of M_n for this realization, is constructed. In this way, the Linear Oracle is constructed with the knowledge of the 'future', thus should has the smallest possible prediction errors among all linear estimators. As Figure 2.9 shows, the performances of the Empirical Linear estimator are almost as good as the Linear Oracle both on a single realization and in average, better than the Empirical Harmonic estimator.

Chapter 3

Fluid Dynamics of An Oil Slick Spreading On Flowing Water

After an oil spill accident happens, the spilled oil is spreading on the sea under the effect of water waves. Based upon the complexity of the dynamics of the underlying water flow, the spreading and evolution process of the oil can be complicated. In this chapter, we will address a reduced model that captures the local dynamics of an oil slick spreading on a flowing water surface and discuss its applications in different scenarios.

3.1 Motivation and A Reduced Model

When an oil slick is spreading on a water surface, other physical process such as evaporation and dissolution can also happen at the same time. In a two dimensional setup, let's denote the thickness of the oil slick as $h(x,t)$ and its velocity as $q(x,t)$.

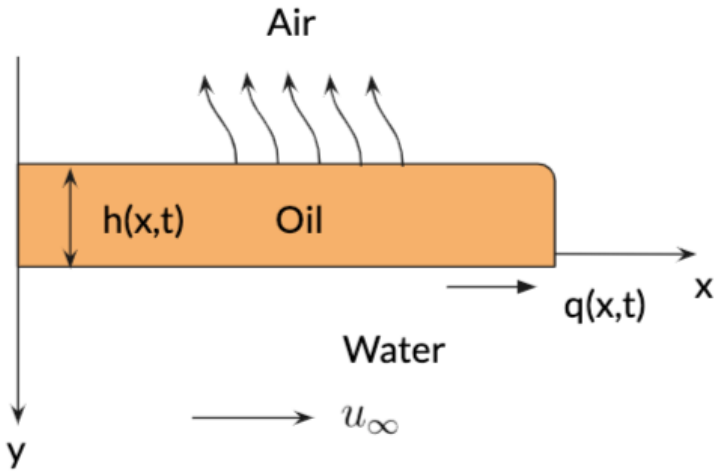

Figure 3.1: Two dimensional setup of an oil slick spreading on a flowing water surface with evaporation

By continuity,

$$\frac{\partial h}{\partial t} + \frac{\partial (qh)}{\partial x} = -\alpha h + \beta \tag{3.1.1}$$

where α is the evaporation rate of the oil, β is other sources. With the 'no-slip' assumption, the velocity of the slick q is the same as the velocity of the water at the surface. Due to the viscous drag, the velocity of the water at the surface is different from the water free stream velocity u_∞. Without loss of generality, we can represent q as

$$q = u_\infty + f \tag{3.1.2}$$

where f is a correction function. Using the representation (3.1.2) for q, the continuity equation (3.1.1) can be written as

$$\frac{\partial h}{\partial t} + \underbrace{u_\infty \frac{\partial h}{\partial x}}_{\text{advection}} = \underbrace{-F(h, \frac{\partial h}{\partial x}, \frac{\partial u}{\partial x}, \cdots)h}_{\text{spread dynamics}} \underbrace{-\alpha h}_{\text{evaporation}} \underbrace{+\beta}_{\text{source}} \tag{3.1.3}$$

where the function F is result from the correction function f for q and it potentially depends on the thickness of the slick, the gradient of the thickness, the stream rate of the water flow and so on. Assuming that the evaporation rate α is constant, the free stream of the water flow u_∞ can be obtained from other models, and the source term β is known, we would be able to model the evolution of the slick thickness once the function F is specified. We will refer to equation (3.1.3) as a reduced model for the oil dynamics on a flowing water surface.

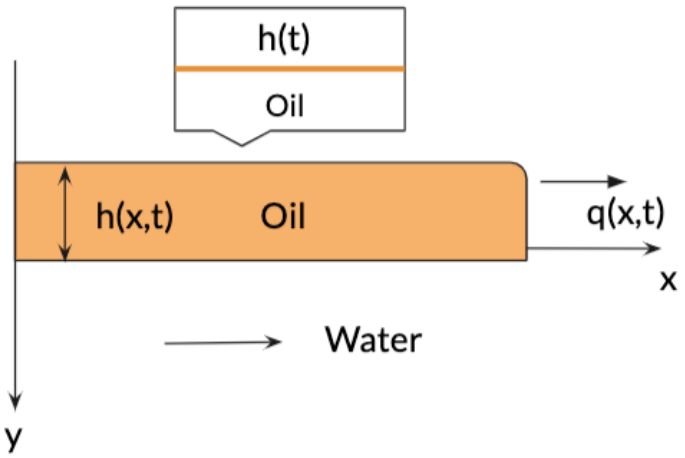

Figure 3.2: The local picture of an oil slick spreading on flowing water surface

Although to characterize the function F for the global phase may be difficult, we can still specify F for the local dynamics. Suppose that (1) the oil slick is nearly flat locally so that its thickness is independent of x, i.e. $h(x,t) = h(t)$ and (2) in a locally moving frame, the stream rate of the horizontal water flow is independent of

x. Therefore, by Taylor expansion approximation, the local horizontal water stream is nearly linear in space, i.e.

$$u = u_0 + \frac{\partial u}{\partial x}x + O(x^2) \approx \eta x, \tag{3.1.4}$$

where $\eta(y,t) = \frac{\partial u}{\partial x}$ is the stream rate of the water flow. Under these assumptions, the continuity equation yields

$$\begin{aligned} &\frac{\partial h}{\partial t} + \frac{\partial (qh)}{\partial x} = -\alpha h + \beta \\ \Rightarrow &\frac{\partial h}{\partial t} = -\eta_0(t)h - \alpha h + \beta \end{aligned} \tag{3.1.5}$$

Comparing the above equation to the reduced model (3.1.3), it suggests that the water stream rate at the surface η_0 shall serve as the function F in a locally moving frame.

Furthermore, the stream rate of the water flow is determined by the unsteady Navier-Stokes equations:

$$\frac{\partial \mathbf{u}}{\partial t} + \mathbf{u}\cdot\nabla\mathbf{u} - \nu_w \Delta \mathbf{u} = -\nabla p \tag{3.1.6}$$

$$\nabla \cdot \mathbf{u} = 0 \tag{3.1.7}$$

which can also be written in terms of η:

$$\frac{\partial \eta}{\partial t} + \eta^2 + v\frac{\partial \eta}{\partial y} - \nu_w \frac{\partial^2 \eta}{\partial y^2} = -\frac{\partial^2 p}{\partial x^2} \tag{3.1.8}$$

Next, we will discuss the solution behaviors of η_0 with three different underlying flows: steady water flow, contracting water flow and expanding water flow.

3.2 Oil Spreading on Unidirectional Contracting Water Surface

When $\frac{\partial u_\infty}{\partial x} < 0$, the underlying water is flowing in the direction towards the center of the oil slick so that the water flow is contracting. For simplicity, let's assume the water stream is contracting to the origin with a velocity linear in space, i.e.

$$u_{\text{free}} = -\eta_\infty x, \quad v_{\text{free}} = \eta_\infty y$$

where $\eta_\infty := |\frac{\partial u_\infty}{\partial x}| > 0$ is independent of x. In this scenario, since the water stream flows in the opposite direction of the oil slick tends to spread, one can expect that the

viscous drag from water acts a more significant dragging effect on the oil slick than the viscous drag inside the oil and the oil inertial force. The gravitational force from the slick itself is more significant on driving it to spread than the net surface tension in a reasonable large time scale. Therefore, the approximated momentum equation for the oil slick is derived from a balance between the water viscous drag force and the oil gravitational force, which is the same as in the 'Viscous' regime of the steady water scenario. A full PDE model that describes the dynamics can be seen as:

$$\frac{\partial h}{\partial t} + \frac{\partial (qh)}{\partial x} = 0 \tag{3.2.1}$$

$$g\Delta h \frac{\partial h}{\partial x} = \nu_w \frac{\partial u}{\partial y}(x, 0; t) \tag{3.2.2}$$

$$\frac{\partial u}{\partial t} + u\frac{\partial u}{\partial x} + v\frac{\partial u}{\partial y} - \nu_w \frac{\partial^2 u}{\partial y^2} = -\frac{\partial p}{\partial x} \tag{3.2.3}$$

$$\frac{\partial v}{\partial t} + u\frac{\partial v}{\partial x} + v\frac{\partial v}{\partial y} - \nu_w \frac{\partial^2 v}{\partial y^2} = -\frac{\partial p}{\partial y} \tag{3.2.4}$$

$$\frac{\partial u}{\partial x} + \frac{\partial v}{\partial y} = 0 \tag{3.2.5}$$

with B.C. that reflects 'no-slip' at the oil-water interface and the contracting free stream

$$\begin{aligned} &u(x, 0; t) = q(x; t), \quad v(x, 0; t) = 0 \\ &\lim_{y\to\infty} u(x, y; t) = -\eta_\infty x \end{aligned} \tag{3.2.6}$$

This time we need to consider a pressure $p(x, y)$ in the water boundary equations that drives the water flows. Right after an oil slick is released from the rest, it tends to spread at a relatively fast speed due to gravity. After a certain amount of time, as the oil slick spreads out, it becomes more flat as a thin layer so that the gravitational driving force decreases. On the other side, the shear stress on the water surface gradually increases due to the increasing oil speed, resulting in an increasing dragging force from the water. Once the gravitational force is balanced by the viscous drag from water, the oil slick reaches a steady state. The order of the steady state can be calculated roughly by an order of magnitude analysis. By simply balancing the orders of the two forces on the left and right sides of equation (3.2.2), we get a reduced ODE:

$$\begin{aligned} g\Delta\frac{h^2}{l} &\sim \nu_w^{\frac{1}{2}} l^{-\frac{1}{2}} (\dot{l} + \eta l)^{\frac{3}{2}} \\ \Rightarrow \dot{l} &\sim (g\Delta V^2 \nu_w^{-\frac{1}{2}})^{\frac{2}{3}} l^{-\frac{5}{3}} - \eta l, \end{aligned} \tag{3.2.7}$$

$$\Rightarrow \dot{l} \quad \text{is} \begin{cases} > 0, & l < (g\Delta V^2)^{\frac{1}{4}} \nu_w^{-\frac{1}{8}} \eta^{-\frac{3}{8}} \\ < 0, & l > (g\Delta V^2)^{\frac{1}{4}} \nu_w^{-\frac{1}{8}} \eta^{-\frac{3}{8}} \end{cases}$$

Thus l has a stable steady state at $l \sim (g\Delta V^2)^{\frac{1}{4}} (\nu_w \eta^3)^{-\frac{1}{8}}$.

More precisely, we can solve for the stationary solution of the full PDE system (3.2.1)-(3.2.5) analytically subject to boundary conditions (3.2.6). Let's seek a stationary solution in the form

$$u(x,y) = -\eta_\infty x f(y\sqrt{\frac{\eta_\infty}{\nu_w}}) \tag{3.2.8}$$

To satisfy the incompressible condition (3.2.5), the water velocity in the vertical direction must be in the form of

$$v(x,y) = \eta_\infty \sqrt{\frac{\nu_w}{\eta_\infty}} g(y\sqrt{\frac{\eta_\infty}{\nu_w}}) \tag{3.2.9}$$

where the function g satisfies $g'(s) = f(s)$. At a steady state, the water flow satisfies the equations

$$u\frac{\partial u}{\partial x} + v\frac{\partial u}{\partial y} - \nu_w \frac{\partial^2 u}{\partial y^2} = -\frac{\partial p}{\partial x} \tag{3.2.10}$$

$$u\frac{\partial v}{\partial x} + v\frac{\partial v}{\partial y} - \nu_w \frac{\partial^2 v}{\partial y^2} = -\frac{\partial p}{\partial y} \tag{3.2.11}$$

Substituting u and v into the above equations yields:

$$\eta_\infty^2 x((g')^2 - gg'' + g''') = -p_x \tag{3.2.12}$$

$$\sqrt{\nu_w \eta_\infty^3}(gg' - g'') = -p_y \tag{3.2.13}$$

From equation (3.2.13) we see $p_{yx} = 0$. So taking the derivative with respect to y on both sides of equation (3.2.12) gives

$$\eta_\infty^2 x \frac{\partial}{\partial y}((g')^2 - gg'' + g''') = 0$$

$$\Rightarrow (g')^2 - gg'' + g''' = C \tag{3.2.14}$$

where C is a constant. We can determine C with the help of the boundary condition

$$\lim_{s\to\infty} g'(s) = 1 \tag{3.2.15}$$

Lemma 1. *If $g'(s) \to 1$ as $s \to \infty$, then $gg'' \to 0$ as $s \to \infty$*

Proof. Assume $\lim_{x\to+\infty} g'(x) = 1$. Now suppose that $\lim_{x\to\infty} \inf gg'' = K > 0$. Because $g' \to 1$, there exists $x_0 > 0$ s.t. $\forall x \geq x_0$, $g'(x) \geq 1 - K/2$. Then for $x \geq x_0$, we have

$$\begin{aligned}
(g')^2 + gg'' &\geq (1 - K/2)^2 + K = 1 + K^2/4 \\
&\Rightarrow (gg')' \geq 1 + K^2/4 \\
&\Rightarrow gg' \geq (1 + K^2/4)x + C_1 \\
&\Rightarrow (\frac{g^2}{2})' \geq (1 + K^2/4)x + C_1 \\
&\Rightarrow g \geq x\sqrt{1 + K^2/4} + C_1\sqrt{x} + C_2 > x
\end{aligned}$$

which contradicts the fact that $g' \to 1$. Therefore $\lim_{x\to+\infty} gg'' = 0$ □

Then taking the limit on both sides of equation (3.2.16) and realizing $g''' \to 0$ gives

$$C = \lim_{x\to\infty} (g')^2 - \lim_{x\to+\infty} gg'' + \lim_{x\to\infty} g''' = 1$$

In the end, we get the equation for the function g

$$(g')^2 - gg'' + g''' = 1 \tag{3.2.16}$$

By the 'no-slip' boundary condition, the water velocity at the oil-water interface $u(x, 0) = q(x) = 0$ and $v(x, 0) = 0$ provide initial conditions for g:

$$g(0) = 0, \quad g'(0) = 0 \tag{3.2.17}$$

Next, we will explore the existence of solutions to ODE (3.2.16) subject to boundary conditions (3.2.15) and (3.2.17). Let $g(s) = s + \xi(s)$. In order to satisfy the boundary condition $\lim_{s\to\infty} g'(s)$=1, ξ must satisfy $\lim_{s\to\infty} \xi'(s) = 0$. Substituting ξ into equation (3.2.16) and neglecting higher order terms yields:

$$\begin{aligned}
(1 + \xi')^2 - (s + \xi)\xi'' + \xi''' &= 1 \\
\Rightarrow 2\xi' - s\xi'' + \xi''' &= 0
\end{aligned} \tag{3.2.18}$$

The general solution to above equation takes the form:

$$\xi'(s) = c_1(s^2 - 1) + c_2(\sqrt{2\pi}(s^2 - 1)\text{erfi}(\frac{s}{\sqrt{2}}) - 2e^{\frac{s^2}{2}}s) \tag{3.2.19}$$

where the imaginary error function erfi(z) has series about infinity

$$\text{erfi}(z) = -i + \frac{e^{z^2}}{\sqrt{\pi}}(z^{-1} + \frac{1}{2}z^{-3} + \frac{3}{4}z^{-5} + \frac{15}{8} + z^{-7} + \cdots) \tag{3.2.20}$$

Thus the series expansion of the solution $\xi'(s)$ about infinity is

$$\begin{aligned}\xi'(s) =& c_1(s^2-1) + c_2(\sqrt{2\pi}s^2\text{erfi}(\frac{s}{\sqrt{2}}) - 2e^{\frac{s^2}{2}}s - \sqrt{2\pi}\text{erfi}(\frac{s}{\sqrt{2}})) \\ =& c_1(s^2-1) + c_2(-\sqrt{2\pi}(s^2-1)i + \sqrt{2}e^{\frac{s^2}{2}}((\frac{s}{\sqrt{2}})^{-3} + (\frac{s}{\sqrt{2}})^{-5} + \cdots)\end{aligned}$$

The asymptotic solution for $\xi'(s)$ contains two independent terms, both are growing towards infinity. Thus the condition $\xi \to 0$ requires both c_1 and c_2 equal to zero. Therefore, the boundary condition (3.2.15) is in fact placing two restrictions on the equation. Along with conditions (3.2.17), a total of four conditions are placed on the third order equation for function g, which force no solutions that exist. A comparable situation is seen in the analysis for the steady water scenario. Buckmaster [2] finds that the asymptotic similarity solution to the original water boundary layer equation consists of two independent terms, both of which can satisfy boundary conditions induced from the original model. However, only a right choice of an extra condition on the water velocity field can lead to a solution that is physically realistic.

To find an extra condition that is indicated by the dynamics, let's consider the vertical change of the horizontal velocity, i.e. $\frac{\partial u}{\partial y}$, within the boundary layer. For an oil slick that is sliding over a water surface that flows in the opposite direction, the water flows near the water surface on top slow down due to the drag of the oil, while the water flow at the bottom of the boundary layer has relatively faster velocity in the negative direction, close to the free stream velocity. Therefore, a physically realistic solution $u(x, y)$ should be monotonically decreasing in the vertical direction in the entire field, or equivalently $\frac{\partial u}{\partial y} \leq 0$ for all $y \geq 0$. By solution (3.2.8),

$$\begin{aligned}& u(x,y) = -\eta_\infty x f(y\sqrt{\frac{\eta_\infty}{\nu_w}}) \\ & \Rightarrow \frac{\partial u}{\partial y} = -\eta_\infty\sqrt{\frac{\eta_\infty}{\nu_w}}xf' = -\eta_\infty\sqrt{\frac{\eta_\infty}{\nu_w}}xg'' \leq 0 \\ & \Rightarrow g''(s) \geq 0, \quad \text{for} \quad s > 0\end{aligned} \tag{3.2.21}$$

Therefore, we will seek for a solution to the equation (3.2.16) subject to conditions $g'(0) = 0$, $\lim_{s\to\infty} g'(s) = 1$ and also satisfies $g''(s) \geq 0$. Approximation of such a solution given by the MATLAB solver bvp4c() is in Figure 3.3.

Then the oil thickness h(x) at the steady state can be solved from the momentum equation (3.2.2):

$$g\Delta h\frac{\partial h}{\partial x} = \nu_w\frac{\partial u}{\partial y}(x, 0; t)$$

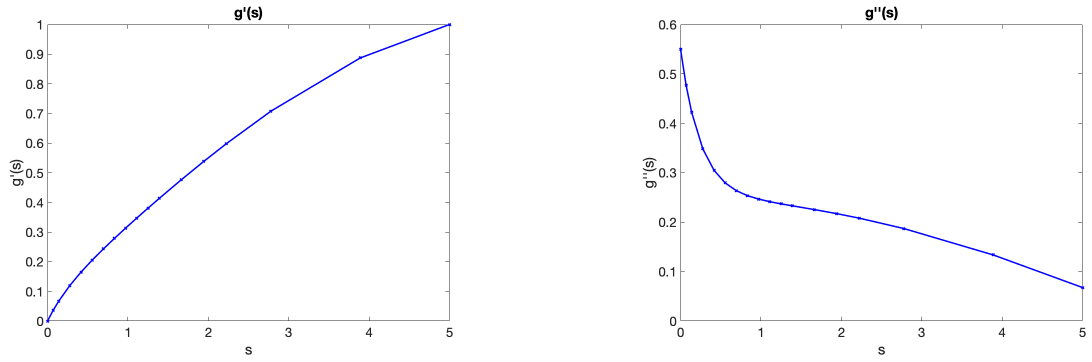

(a) (b)

Figure 3.3: Approximations of (a) g'(s) and (b) g"(s) by MATLAB

$$\Rightarrow g\Delta\frac{\partial}{\partial x}(\frac{1}{2}h^2) = -\eta_\infty^{\frac{3}{2}}\nu_w^{\frac{1}{2}}xg''(0)$$

$$\Rightarrow h^2 = h^2(0) - \frac{\eta_\infty\sqrt{\eta_\infty\nu_w}}{g\Delta}g''(0)x^2 \tag{3.2.22}$$

where $g''(0) \approx 0.55$ referring to Figure 3.3b. Since we assume a constant volume V of oil is conserved, the radius of the oil layer at the steady state R_s can be calculated from

$$\int_0^{R_s} h(x)dx = \frac{V}{2}$$

3.3 Oil Spreading on Unidirectional Expanding Water Surface

In another circumstance, when $\frac{\partial u_\infty}{\partial x} > 0$, the oil slick is spreading on a water surface with a flow in the direction towards the edge of the oil. The spread is expected to be faster than spreading on a steady water surface. In the following part, we will analyze the dynamics of the oil spreading process on a flowing stream, whose velocity is linearly expanded over space, i.e.

$$u_{\text{free}} = \eta_\infty x, \quad v_{\text{free}} = -\eta_\infty y$$

where $\eta_\infty = |\frac{\partial u_\infty}{\partial x}| > 0$ is independent of x. In this circumstance, the water flow always travels in the direction towards the edge of the slick at a faster speed so that it pushes the slick to spread.

Inspired by Buckmaster's method [2], let's first derive the full momentum equation for an oil slick on a flowing water surface. Similar to the steady water scenario, there are still four forces that are involved in this dynamics. As before, the gravitational

force is promoting the oil to spread. But instead of always dragging the spreading in the steady water case, the viscous drag from the water now can either drag or drive the oil spreading, depending on the velocity of the underlying water flow. On the other side, the viscous drag inside the oil and the inertial force are the two forces that retards the spreading. Considering the small magnitude of the net surface tension from the real measurement shown in Table 2.2, we will neglect the surface tension effect for the time scale we are interested in.

We start with driving the term of viscous drag inside the oil. Let's use A to denote the thickness of the slick part that is floating above the water surface and B to denote the thickness of the part below water surface. By buoyancy balance, $B = \Delta h$. Use this in the continuity equation, we have,

$$\dot{B} = (A + B)\frac{\partial q}{\partial x} + \dot{A} = h\frac{\partial q}{\partial x} + \Delta\dot{h}$$

The viscous drag inside the oil can then be computed by the shear stress:

$$\nu_o \frac{\partial(\dot{B})}{\partial x} = \nu_o \frac{\partial}{\partial x}(h\frac{\partial q}{\partial x} + \Delta\dot{h}) \approx \nu_o \frac{\partial}{\partial x}(h\frac{\partial q}{\partial x}) \tag{3.3.1}$$

known that $\Delta \ll 1$.

Next, the inertial force is given by Newton's Law,

$$h\frac{Dq}{Dt} = h(\frac{\partial q}{\partial t} + q\frac{\partial q}{\partial x}) \tag{3.3.2}$$

In a moving coordinate frame which is set at the center of the oil slick, the gravitational term and the viscous drag term from water are the same as in the Buckmaster's model. Thus the full momentum equation for an oil slick on a flowing water surface is

$$-g\Delta h\frac{\partial h}{\partial x} + \nu_w \frac{\partial u}{\partial y}(x, 0; t) = -\nu_o \frac{\partial}{\partial x}(h\frac{\partial q}{\partial x}) + h(\frac{\partial q}{\partial t} + q\frac{\partial q}{\partial x}) \tag{3.3.3}$$

The fact that whether the viscous drag from water is promoting or retarding the oil spreading is determined by the sign of the shear stress $\frac{\partial u}{\partial y}(x, 0; t)$.

Recall that for a bulk model that we are using for the oil slick, we assume a hydrostatic equilibrium inside the oil, which implies that the effect of the viscous drag inside the oil can be neglected. Here we can justify this assumption by comparing the order of magnitude of the viscous drag from oil with other retarding effect.

On the retarding forces side, the order of magnitude of the viscous drag from the oil can been seen from its expression (3.3.1), which is of $\nu_o h l^{-1} t^{-1}$. While the inertial force has the order of hlt^{-2} from the expression (3.3.2). A direct comparison of the two orders gives

$$\frac{hlt^{-2}}{\nu_o h l^{-1} t^{-1}} \sim \frac{l^2}{\nu_o t} \sim (\frac{l}{\sqrt{\nu_o t}})^2 \gg 1, \tag{3.3.4}$$

which suggests that the effect of the viscous drag inside the oil is indeed negligible, comparing to the effect of inertia. Thus, we can simply the full momentum equation by dropping the oil viscous drag term to get

$$-g\Delta h\frac{\partial h}{\partial x} + \nu_w \frac{\partial u}{\partial y}(x,0;t) = h(\frac{\partial q}{\partial t} + q\frac{\partial q}{\partial x}) \tag{3.3.5}$$

The system of equations that governs this process is

$$\frac{\partial h}{\partial t} + \frac{\partial (qh)}{\partial x} = 0 \tag{3.3.6}$$

$$-g\Delta h\frac{\partial h}{\partial x} + \nu_w \frac{\partial u}{\partial y}(x,0;t) = h(\frac{\partial q}{\partial t} + q\frac{\partial q}{\partial x}) \tag{3.3.7}$$

$$\frac{\partial u}{\partial t} + u\frac{\partial u}{\partial x} + v\frac{\partial u}{\partial y} - \nu_w \frac{\partial^2 u}{\partial y^2} = -\frac{\partial p}{\partial x} \tag{3.3.8}$$

$$\frac{\partial v}{\partial t} + u\frac{\partial v}{\partial x} + v\frac{\partial v}{\partial y} - \nu_w \frac{\partial^2 v}{\partial y^2} = -\frac{\partial p}{\partial y} \tag{3.3.9}$$

$$\frac{\partial u}{\partial x} + \frac{\partial v}{\partial y} = 0 \tag{3.3.10}$$

with boundary conditions

$$u(x,0;t) = q(x,t), \quad v(x,0;t) = 0 \tag{3.3.11}$$

$$\lim_{y\to\infty} u(x,y;t) = \eta_\infty x \tag{3.3.12}$$

Motivated by Fay's analysis for the steady water case [8, 9], we can derive an approximation of the spreading law for this flowing water case through an order of magnitude analysis. The order of the gravitational force is the same as before $g\Delta h^2 l^{-1}$ The order of the water viscous drag is characterized by the time variant of the length scale l, as $\nu_w^{\frac{1}{2}} l^{-\frac{1}{2}} (\eta_\infty l - \dot{l})^{\frac{3}{2}}$. And the order of the inertial force is approximated by $h\ddot{l}$, with a drop of the advection effect due to its small impact. A direct balance between the orders of magnitude of promoting and retarding forces gives an ODE:

$$\nu_w^{\frac{1}{2}} l^{-\frac{1}{2}} (\eta_\infty l - \dot{l})^{\frac{3}{2}} \sim h\ddot{l} + g\Delta h^2 l^{-1}$$

$$\Rightarrow V l^2 \ddot{l} - \nu_w^{\frac{5}{2}} l^{\frac{1}{2}} (\eta_\infty l - \dot{l})^{\frac{3}{2}} + g\Delta V^2 \sim 0 \tag{3.3.13}$$

If we propose an exponential solution $l \sim e^{\alpha t}$ to this balance equation, we get

$$V\alpha^2 e^{3\alpha t} - \nu_w^{\frac{1}{2}} e^{4\alpha t}(\eta_\infty - \alpha)^{\frac{3}{2}} + g\Delta V^2 \sim 0 \tag{3.3.14}$$

The leading order term suggests that $\alpha \to \eta_\infty$ as $t \to \infty$. Therefore, we can infer that the asymptotic spreading law of on oil slick on a linear water flow is $l \sim e^{\eta_\infty t}$, where η_∞ is the horizontal free stream rate of the underlying water flow.

Analytically, we will seek for a quasi-steady solution for the PDE system (3.3.6) - (3.3.10) subject to the boundary conditions (3.3.11) and (3.3.12). As in the contracting water flow case, we are still looking for a solution in the forms of

$$u(x,y) = -\eta_\infty x f(y\sqrt{\frac{\eta_\infty}{\nu_w}}) \tag{3.3.15}$$

$$v(x,y) = \eta_\infty \sqrt{\frac{\nu_w}{\eta_\infty}} g(y\sqrt{\frac{\eta_\infty}{\nu_w}}) \tag{3.3.16}$$

where the function g satisfies $g'(s) = f(s)$. At a quasi-steady state, the water flow satisfies the steady Navier-Stokes equations

$$u\frac{\partial u}{\partial x} + v\frac{\partial u}{\partial y} - \nu_w \frac{\partial^2 u}{\partial y^2} = -\frac{\partial p}{\partial x} \tag{3.3.17}$$

$$u\frac{\partial v}{\partial x} + v\frac{\partial v}{\partial y} - \nu_w \frac{\partial^2 v}{\partial y^2} = -\frac{\partial p}{\partial y} \tag{3.3.18}$$

Substituting u and v into the above equations and following the same steps as in the contracting water flow case yields the same ODE satisfied by g:

$$(g')^2 - gg'' + g''' = 1 \tag{3.3.19}$$

The free stream boundary condition on u (3.3.12) now yields

$$\lim_{s\to\infty} g'(s) = -1 \tag{3.3.20}$$

For the 'no-slip' boundary conditions at the oil-water interface (3.3.11), we discard the condition $v(x,0;t) = 0$ because of the same reason as in the contracting water flow case. The condition on the horizontal velocity $u(x,0;t) = q(x,t)$ together with the oil momentum equation (3.3.7) exposes the other condition on function g. Ignoring the gravitational driving, the momentum equation for the oil is

$$\nu_w \frac{\partial u}{\partial y}(x,0;t) = h(\frac{\partial q}{\partial t} + q\frac{\partial q}{\partial x}) \tag{3.3.21}$$

Substitution of the solution form (3.3.15) for u and replace q with $u(x,0;t)$ result in

$$g''(0) = -h\eta_\infty^{\frac{1}{2}} \nu_w^{-\frac{1}{2}} [g'(0)]^2 \tag{3.3.22}$$

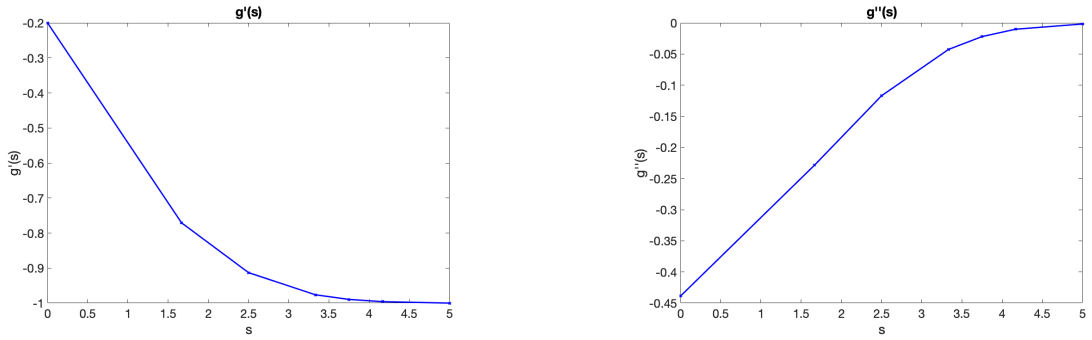

(a) (b)

Figure 3.4: Approximations of (a) g'(s) and (b) g"(s) by MATLAB

Hence, the quasi-steady state solution of the PDE system (3.3.6) - (3.3.12) is determined by the solution of the ODE (3.3.19) subject to boundary conditions (3.3.20) and (3.3.22). Since condition (3.3.22) depends on the slick thickness h, the solution of g is a function of h. Considering that in this regime of spreading, the slick thickness changes slowly in a local frame, we can solve for a solution $g(s)$ satisfying the condition (3.3.22) for a fixed value of h.

When looking for a solution of g numerically, we realize the physical fact that the horizontal velocity u now increases in the vertical direction due to the viscous drag and a faster expanding free stream velocity. So

$$\begin{aligned} & u(x,y) = -\eta_\infty x f(y\sqrt{\frac{\eta_\infty}{\nu_w}}) \\ & \Rightarrow \frac{\partial u}{\partial y} = -\eta_\infty\sqrt{\frac{\eta_\infty}{\nu_w}} x f' = -\eta_\infty\sqrt{\frac{\eta_\infty}{\nu_w}} x g'' \geq 0 \\ & \Rightarrow g''(s) \leq 0, \quad \text{for} \quad s > 0 \end{aligned} \tag{3.3.23}$$

As an example, the numerical solutions of $g'(s)$ and $g''(s)$ solved for $h\eta_\infty^{\frac{1}{2}}\nu_w^{-\frac{1}{2}} = 11$ are shown in 3.4a and 3.4b, which suggest $g'(0) \approx -0.2$. The corresponding stream rate at the surface $\eta_0(t,y)$ is then

$$\eta_0(y,t) = -\eta_\infty g'(0) = 0.2\eta_\infty \tag{3.3.24}$$

3.4 A Numerical Simulation of the Viscous Spreading On Calm Water Surface

Following the order of magnitude analysis by Fay [8] and Hoult [14], while an oil slick is spreading on steady water and in the 'Viscous' regime, its radius should spread at

a rate of $t^{\frac{3}{8}}$. Furthermore, Buckmaster derived a system of equations that governs the dynamics of the spreading in this regime for the two dimensional setup [2]. The equations are the following:

$$\frac{\partial h}{\partial t} + \frac{\partial (qh)}{\partial x} = 0 \tag{3.4.1}$$

$$-\frac{\nu_w}{g\Delta}\frac{\partial u}{\partial y}(x,0;t) + h\frac{\partial h}{\partial x} = 0 \tag{3.4.2}$$

$$\frac{\partial u}{\partial t} + u\frac{\partial u}{\partial x} + v\frac{\partial u}{\partial y} = \nu_w \frac{\partial^2 u}{\partial y^2} \tag{3.4.3}$$

$$\frac{\partial u}{\partial x} + \frac{\partial v}{\partial y} = 0 \tag{3.4.4}$$

with the 'no-slip' boundary conditions

$$u(x,0;t) = q(x,t), \quad v(x,0;t) = 0 \tag{3.4.5}$$

$$\lim_{y\to\infty} u(x,y;t) = 0 \tag{3.4.6}$$

$$q(R(t),t) = \dot{R}(t) \tag{3.4.7}$$

where $h(x;t)$ is the thickness of the oil layer, $q(x;t)$ is the velocity of the oil, $u(x,y;t)$ is the velocity of the water underneath the oil layer and $R(t)$ is the radius of the oil.

Buckmaster obtains an approximate solution of this PDE systems. The analysis yields that the velocity of the oil is

$$q(x;t) = \frac{3}{8}\frac{x}{t}$$

Therefore, the stream rate of the water flow at the surface is:

$$\eta_0 = \frac{3}{8t} \tag{3.4.8}$$

The radius of the oil slick is indeed spreading at the rate of $t^{\frac{3}{8}}$ and the approximate spreading law is solved through a series expansion of the solution to the system of PDEs (3.4.1) - (3.4.7), as:

$$R(t) = 1.76(g\Delta)^{\frac{1}{4}} V^{\frac{1}{2}} \nu_w^{-\frac{1}{8}} t^{\frac{3}{8}}$$

We develop a numerical solver that simulates the dynamics of the oil slick spreading on a calm water surface and validate the schemes using Buckmaster's analysis. In a summary, we will solve the system of equations (3.4.1) - (3.4.3) in the following order:

1. Assuming that at a certain fixed time point, the instantaneous thickness of the oil layer can be measured by some means. We will use this measurement as the initial state $h_0(x) = h(x; 0)$.

2. The evolution of the thickness h can then be determined by the continuity equation (3.4.1).

3. Once the thickness h at the next time is known, it can be used in the momentum equation (3.4.2) to computed the shear stress $\frac{\partial u}{\partial y}(x, 0; t)$ for that moment.

4. The resulting shear stress will then be implemented in the boundary-layer equation (3.4.3) as the boundary conditions to update the underlying water velocity.

5. The oil velocity q will then be assigned by the water velocity at the surface, according to the 'no-slip' boundary condition.

Now we will present the details of the numerical schemes that we use to solve each of the equations. In the following part that describes the numerical schemes, the superscript represents the time step index and the subscript represents the spatial index, and δx, δy, δt are the spatial and time discretization sizes, respectively.

In particular, starting from an initial state $h^0(x)$ and $q^0(x) = 0$, we first use the Lax-Friedrichs scheme [7] to solve h^{n+1} from the continuity equation (3.4.1):

$$h_j^{n+1} = \frac{1}{2}(h_{j+1}^n + h_{j-1}^n) - \frac{\delta t}{2\delta x}(q_{j+1}^n h_{j+1}^n - q_{j-1}^n h_{j-1}^n) \tag{3.4.9}$$

The Lax-Friedrichs method is explicit and first order accurate in time and second order accurate in space ($O(\delta t) + O(\frac{\delta x^2}{\delta t})$). The method is stable if and only if the the Courant-Friedrichs-Leway (CFL) condition [5] is satisfied:

$$|q\frac{\delta t}{\delta x}| \leq 1$$

To deal with the discretization at the boundaries, recall that in the coordinate frame that is set at the center of the slick, the center does not move ($q(0; t) = 0$) and the spreading dynamics is symmetric about the center so that we can assign $q_{-1} = -q_1$ and $h_{-1} = h_1$.

Next we use h_i^{n+1} to compute the shear stress $s_i^{n+1} := [\frac{\partial u}{\partial y}(x, 0)]^{n+1}$ through the momentum equation (3.4.2).

$$s_j^{n+1} = [\frac{\partial u}{\partial y}(x, 0)]^{n+1} = \frac{g\Delta}{\nu_w}\frac{1}{2}\frac{(h_{j+1}^{n+1})^2 - (h_j^{n+1})^2}{\delta x} \tag{3.4.10}$$

A first order forward method is being used to approximate the spatial derivatives $h\frac{\partial h}{\partial x}$ with $O(\delta x)$ accuracy in space.

Then the velocity of the underlying water u^{n+1} will be computed from the water flow equation (3.4.3). We will split this step into two mini steps, each dealing with the diffusion and advection effects separately. We first update an intermediate state $u^{n+\frac{1}{2}}$ that is only caused by the diffusion effect $\frac{\partial u}{\partial t} = \nu_w \frac{\partial^2 u}{\partial y^2}$ using the Crank-Nicolson method [6]:

$$u_{i,j}^{n+\frac{1}{2}} - r(u_{i+1,j}^{n+\frac{1}{2}} - 2u_{i,j}^{n+\frac{1}{2}} + u_{i-1,j}^{n+\frac{1}{2}}) = u_{i,j}^{n} + r(u_{i+1,j}^{n} - 2u_{i,j}^{n} + u_{i-1,j}^{n}), \quad i = 2, 3, ..., N \tag{3.4.11}$$

where $r = \frac{\nu \delta t}{4 \delta y^2}$. At the water-oil interface i.e. i=1, the shear stress yielded from (3.4.10) will be specified as the boundary condition and be used to update the velocity

$$u_{1,j}^{n+\frac{1}{2}} - r(u_{2,j}^{n+\frac{1}{2}} - u_{1,j}^{n+\frac{1}{2}}) = u_{1,j}^{n} + r(u_{2,j}^{n} - u_{1,j}^{n}) - r(\delta y) s_j^{n+\frac{1}{2}} - r(\delta y) s_j^{n} \tag{3.4.12}$$

The Crank-Nicolson method is second order accurate in time and it is unconditionally stable [26] for the diffusion equation.

We then update the intermediate state $u^{n+\frac{1}{2}}$ half a step further under the effect of horizontal advection and neglect the vertical advection. A simplified advection equation $\frac{\partial u}{\partial t} + u \frac{\partial u}{\partial x} = 0$ is solved for u^{n+1}, using the Upwind method [20] :

$$u_j^{n+1} = \begin{cases} u_j^{n+\frac{1}{2}} - u_j^{n+\frac{1}{2}} \frac{\delta t}{2 \delta x} (u_j^{n+\frac{1}{2}} - u_{j-1}^{n+\frac{1}{2}}), & \text{if} \quad u_j > 0 \\ u_j^{n+\frac{1}{2}} - u_j^{n+\frac{1}{2}} \frac{\delta t}{2 \delta x} (u_{j+1}^{n+\frac{1}{2}} - u_j^{n+\frac{1}{2}}), & \text{if} \quad u_j < 0 \end{cases} \tag{3.4.13}$$

The Upwind scheme is adjusted to coincide the direction of propagation of the traveling waves. The method is first order accurate in space and time and it is stable if the CFL condition holds $|u \frac{\delta t/2}{\delta x}| \leq 1$. Lastly, according to the 'no-slip' boundary condition, we set the oil velocity q^{n+1} to the water velocity at the interface $q^{n+1} = u_1^{n+1}$ to continue the iteration.

Based on this numerical simulation to the PDE model (3.4.1)-(3.4.7), we are able to track the radius growing rate of an oil slick while it is spreading on a steady water surface. A plot of the radius of an oil slick, which is initially in the shape of ellipse, versus time is present in Figure 3.5. The growing curve can be fitted by a straight line with a slope $\frac{3}{8}$ and intercept in the asymptotic sense, indicating that the oil slick is spreading in a behavior of

$$R(t) \sim (g\Delta)^{\frac{1}{4}} V^{\frac{1}{2}} \nu_w^{-\frac{1}{8}} t^{\frac{3}{8}} \tag{3.4.14}$$

The numerical simulation of the 'Viscous' regime for steady water scenario demonstrates Buckmaster's analysis and provides a work flow to numerically simulate the spreading dynamics with more complicated underlying flow. Buckmaster's result on the spreading coefficient differs from the experimental data by approximately 17%.

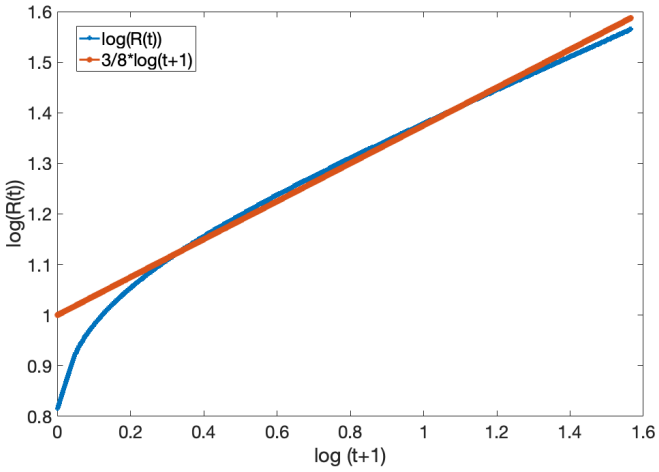

Figure 3.5: Log plot of the oil slick radius vs time

3.5 A Numerical Simulation Of The Spreading On Expanding Water Surface

For an oil slick spreading on a water surface with expanding flow, we want to numerically simulate the dynamics using similar schemes developed for the calm water scenarios.

For simplicity, we take the following system of PDEs and seek for its numerical solution.

$$\frac{\partial h}{\partial t} + \frac{\partial (qh)}{\partial x} = 0 \tag{3.5.1}$$

$$-g\Delta h\frac{\partial h}{\partial x} + \nu_w \frac{\partial u}{\partial y}(x,0;t) = h(\frac{\partial q}{\partial t} + q\frac{\partial q}{\partial x}) \tag{3.5.2}$$

$$\frac{\partial u}{\partial t} + u\frac{\partial u}{\partial x} = \nu_w \frac{\partial^2 u}{\partial y^2} \tag{3.5.3}$$

with boundary conditions

$$u(x,0;t) = q(x,t), \quad \lim_{y\to\infty} u(x,y;t) = \eta_\infty x \tag{3.5.4}$$

A rescaling on the variables can further simplify the equations to

$$\frac{\partial \tilde{h}}{\partial \tilde{t}} + \frac{\partial(\tilde{q}\tilde{h})}{\partial \tilde{x}} = 0 \tag{3.5.5}$$

$$-\tilde{h}\frac{\partial \tilde{h}}{\partial \tilde{x}} + \frac{\partial \tilde{u}}{\partial \tilde{y}}(\tilde{x}, 0; \tilde{t}) = \tilde{h}(\frac{\partial \tilde{q}}{\partial \tilde{t}} + \tilde{q}\frac{\partial \tilde{q}}{\partial \tilde{x}}) \tag{3.5.6}$$

$$\frac{\partial \tilde{u}}{\partial \tilde{t}} + \tilde{u}\frac{\partial \tilde{u}}{\partial \tilde{x}} = \frac{\partial^2 \tilde{u}}{\partial \tilde{y}^2} \tag{3.5.7}$$

with dimensionless variables

$$\begin{aligned} h &= (V\nu_w)^{\frac{2}{7}}(g\Delta)^{-\frac{1}{7}}\tilde{h} \\ x &= V^{\frac{5}{7}}\nu_w^{-\frac{2}{7}}(g\Delta)^{\frac{1}{7}}\tilde{x} \\ y &= (V\nu_w)^{\frac{2}{7}}(g\Delta)^{-\frac{1}{7}}\tilde{y} \\ t &= V^{\frac{4}{7}}\nu_w^{-\frac{3}{7}}(g\Delta)^{-\frac{2}{7}}\tilde{t} \\ u &= V^{\frac{1}{7}}\nu_w^{\frac{1}{7}}(g\Delta)^{\frac{3}{7}}\tilde{u} \\ q &= V^{\frac{1}{7}}\nu_w^{\frac{1}{7}}(g\Delta)^{\frac{3}{7}}\tilde{q} \end{aligned} \tag{3.5.8}$$

It is noted that the time scale in this setup, $V^{\frac{4}{7}}\nu_w^{-\frac{3}{7}}(g\Delta)^{-\frac{2}{7}}$, can be quite big if the volume of the oil slick is massive. Alternatively, on a rather smaller time scale, the rescaling parameter for the gravitational term is much smaller than other terms'. Because of this reason, we will neglect the gravitational term in our simulations.

For simulation, we solve the system of equations (3.5.5)-(3.5.7) numerically using the methods that we implement for the steady water system in section 2.4. Starting from an initial state $h^0(x)$ and $q^0(x) = 0$, we first use the Lax-Friedrichs scheme [7] to solve h^{n+1} from the continuity equation (3.5.5):

$$h_j^{n+1} = \frac{1}{2}(h_{j+1}^n + h_{j-1}^n) - \frac{\delta t}{2\delta x}(q_{j+1}^n h_{j+1}^n - q_{j-1}^n h_{j-1}^n) \tag{3.5.9}$$

For simulation on a short time scale, we will only keep the inertial effect but ignore the gravitational term in the momentum equation. The shear stress $s_j^{n+1} := [\frac{\partial u}{\partial y}(x, 0)]^{n+1}$ will then be expressed in terms of q^n and q^{n+1} according to the oil momentum equation (3.5.6).

$$\begin{aligned} s_j^{n+1} = [\frac{\partial u}{\partial y}(x, 0)]^{n+1} &= h_j^n(\frac{q_j^{n+1} - q_j^n}{\delta t} + \frac{1}{2}\frac{(q_{j+1}^n)^2 - (q_{j-1}^n)^2}{2\delta x}) \\ &= h_j^n(\frac{u_{1,j}^{n+1} - u_{1,j}^n}{\delta t} + \frac{1}{2}\frac{(u_{1,j+1}^n)^2 - (u_{1,j-1}^n)^2}{2\delta x}) \end{aligned} \tag{3.5.10}$$

A same strategy as we used in the steady water model is used to solve for the velocity of the water flow u^{n+1} from the boundary layer equation (3.5.7). We first update an intermediate state $u^{n+\frac{1}{2}}$ effected by the diffusion using the Crank-Nicolson method [6]. For the velocity field under the oil-water surface, the Crank-Nicolson scheme is still written as:

$$u_{i,j}^{n+\frac{1}{2}} - r(u_{i+1,j}^{n+\frac{1}{2}} - 2u_{i,j}^{n+\frac{1}{2}} + u_{i-1,j}^{n+\frac{1}{2}}) = u_{i,j}^{n} + r(u_{i+1,j}^{n} - 2u_{i,j}^{n} + u_{i-1,j}^{n}), \quad i = 2, 3, ..., N \tag{3.5.11}$$

where $r = \frac{\delta t}{4\delta y^2}$. However, at the water-oil interface i.e. i=1, the expression of the shear stress s_j^{n+1} (3.5.10) is used to yield

$$u_{1,j}^{n+\frac{1}{2}} - r(u_{2,j}^{n+\frac{1}{2}} - u_{1,j}^{n+\frac{1}{2}}) = u_{1,j}^{n} + r(u_{2,j}^{n} - u_{1,j}^{n}) - r(\delta y)s_j^{n+\frac{1}{2}} - r(\delta y)s_j^{n} \tag{3.5.12}$$

We then update the intermediate state $u^{n+\frac{1}{2}}$ half a step further with an effect of advection, using the Upwind method [20] :

$$u_i^{n+1} = \begin{cases} u_j^{n+\frac{1}{2}} - u_j^{n+\frac{1}{2}} \frac{\delta t}{2\delta x}(u_j^{n+\frac{1}{2}} - u_{j-1}^{n+\frac{1}{2}}), & \text{if} \quad u_j > 0 \\ u_j^{n+\frac{1}{2}} - u_j^{n+\frac{1}{2}} \frac{\delta t}{2\delta x}(u_{j+1}^{n+\frac{1}{2}} - u_j^{n+\frac{1}{2}}), & \text{if} \quad u_j < 0 \end{cases} \tag{3.5.13}$$

Based on our simulation result shown in Figure 3.6, the magnitude of the gravitational force is no more than 10% and most of the time less than 5% of the magnitude of the water viscous drag, which demonstrates the reliability to neglect the effect of gravitational effect on a short time scale. The simulation result also indicates that the solution to the order balance equation (3.3.13) is converging to the numerical solution solved from the full PDE system asymptotically. And in the example of setting the free stream expanding parameter $\eta_\infty = 1$, both solutions suggest that $R(t) \sim e^{\eta_\infty t}$. Therefore, for simplification purpose, ODE (3.3.13) can be potentially used as a reduced model of the spreading process on a large time scale.

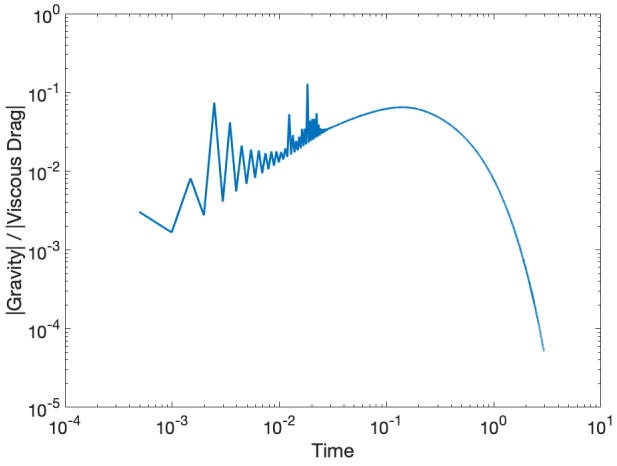

(a)

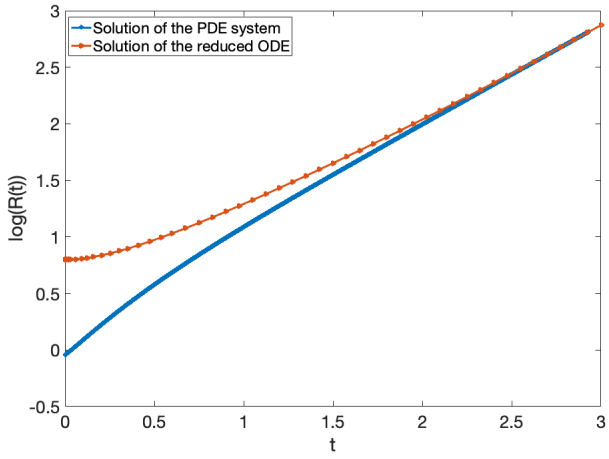

(b)

Figure 3.6: (a) Ratio of gravitational force to water viscous drag. (b) Numerical simulation of the spreading rate verses solution to the reduced ODE

Chapter 4

Multilayer Stochastic Models and Data Assimilation

In the previous chapter, We develop a reduced model that tracks the evolution of an oil slick spreading on a water surface. However, applying such a model to a real scenario is still difficult. In practice, the underlying water can have complicated free stream flows such as oceanic waves. Modeling the dynamics of crude oil is also challenging since a bulk model we addressed will not reflect the dynamics of crude oil accurately, which composes of multiple chemical components. Therefore, we want to develop a statistical framework that integrates the reduced physical model with observable data to produce a reliable estimation of the oil evolution practically.

4.1 A Multilayer Stochastic Model

We first introduce a multilayer stochastic model developed before [27] based on the asymptotic estimator that was derived in section 2.2. The asymptotic estimator (2.2.47) is non-autonomous, because of the result that its estimate coefficients h_j^n depend on actual time n. Since it is difficult to identify the 'true' time associated with oil at a certain state in a real scenario, using the Asymptotic estimator to predict the future evolution of the oil is practically impossible.

An improvement of the Asymptotic estimator is to enlarge its 'phase space' by introducing an additional variable κ into the dynamical system so that the time-dependent system is recast as an autonomous system in the larger phase space. In particular, this means that we parametrize the system as

$$\begin{aligned} M_n &= \sum_{j=1}^{L} h_j^{(\kappa_n)} M_{n-j} + \sigma_n \theta_n \\ \kappa_n &= \kappa_{n-1} + 1 + s\theta_n' \\ \sigma_n &\sim \bar{\sigma}^2 \frac{L!}{\kappa_n^{L+1}} \end{aligned} \tag{4.1.1}$$

In this model, the time influence is reflected by a dynamical variable κ, which is introduced to track the microscopic structure of the oil in terms of its 'age'. The estimator coefficient $h_j^{(\kappa_n)}$ is given by (2.2.45) with n replaced by κ_n. Since the dependence of the parameter h_j on time n has been embed into its dependence on κ, a variable that is a part of the dynamics, this reduced model (4.1.1) is autonomous.

This model is an example of multilayer stochastic model, in which multiple dynamical processes are involved and interact. Typically, one of the variables M_n, referred to as the weighted average concentration of the oil, can be directly observed/measured in practice, while the variable κ_n is a hidden layer that is not observable. Assuming only noisy measurements of M_n are given, one way to estimate both states of (M_n, κ_n) in such a multilayer stochastic model with hidden variables is using the data assimilation methods.

4.1.1 A Brief Review on Kalman Filter Method

In this section, we present a short review of the Kalman Filter [28], one of the data assimilation methods that is widely applied in many fields. Without loss of generality, suppose we have a discrete linear dynamical system:

$$x_{k+1} = Mx_k, \quad k = 0, 1, 2, \cdots \tag{4.1.2}$$

where $x \in \mathbb{R}^n$, and $M \in \mathbb{R}^{n\times n}$, with initial condition $x_0 \sim \mathcal{N}(\mu_0, P_0)$. Assume that a noisy measurement at the next time step y_{k+1} of the following form is valid.

$$y_{k+1} = Hx_{k+1} + \eta_{k+1}$$

where $y_{k+1} \in \mathbb{R}^m$, $H \in \mathbb{R}^{m\times n}$ is a projection from the state space to the observation space and $\eta_{k+1} \sim \mathcal{N}(0, R)$ is an i.i.d. random noise. H does have not to be the identity matrix, meaning that a dynamical variable that is not directly observable is allowed. For the multilayer model (4.1.1) the state space is $(M_n, \kappa_n)^T$, and the observation projection matrix H is $(1, 0)$. Immediately, we have y_{k+1} given x_{k+1} is also a Gaussian random variable:

$$y_{k+1}|x_{k+1} \sim \mathcal{N}(Hx_{k+1}, R)$$

When estimating a dynamical system (4.1.2) with a random Gaussian initial condition, we have

$$x_k|(y_1, y_2, \cdots, y_k) \sim \mathcal{N}(\mu_k, P_k)$$

To predict for the future state x_{k+1}, we would first use the dynamical model to get a 'forecast' mean and variance of x_{k+1}:

$$\mu_f = M\mu_k, \quad P_f = MP_kM^T \tag{4.1.3}$$

The by Bayes' rule,

$$\begin{aligned} P(x_{k+1}|y_{k+1}) &= P(y_{k+1}|x_{k+1})P(x_{k+1}) \\ &\propto \exp\left[-\frac{1}{2}(y_{k+1} - Hx_{k+1})^T R^{-1}(y_{k+1} - Hx_{k+1})\right] \\ &\cdot \exp\left[-\frac{1}{2}(x_{k+1} - \mu_f)^T P_f^{-1}(x_{k+1} - \mu_f)\right] \\ &\propto \exp\left(-F(x_{k+1})\right) \end{aligned}$$

where

$$F(x_{k+1}) = \frac{1}{2}(y_{k+1} - Hx_{k+1})^T R^{-1}(y_{k+1} - Hx_{k+1}) + \frac{1}{2}(x_{k+1} - \mu_f)^T P_f^{-1}(x_{k+1} - \mu_f)$$

is a quadratic function of x_{k+1}. One can show that a distribution with such a pdf function is a Normal distribution with mean $\mu_{k+1} = \arg\min F(x_k)$ and covariance P_{k+1} =inverse of the Hessian of $F(x_k)$. A direct calculation yields

$$\begin{aligned} \nabla F = H^T R^{-1}(Hx_{k+1} - y_{k+1}) + P_f^{-1}(x_{k+1} - \mu_f) = 0 \\ \Rightarrow x^*_{k+1} = (H^T R^{-1} H + P_f^{-1})^{-1}(P_f^{-1}\mu_f + H^T R^{-1} y_{k+1}) \end{aligned}$$

and

$$\begin{aligned} \text{Hess}(F) = H^T R^{-1} H + P_f^{-1} \\ \Rightarrow P_{k+1} = (H^T R^{-1} H + P_f^{-1})^{-1} \end{aligned}$$

With the use of the Woodbury Matrix identity, the mean and variance can further be simplified as

$$\begin{aligned} \mu_{k+1} &= \mu_f + K(y_{k+1} - H\mu_f) \\ P_{k+1} &= (I - KH)P_f \end{aligned} \tag{4.1.4}$$

where I is the identity matrix and $K = P_f H^T (HP_f H^T + R)^{-1}$ is called the 'Kalman gain'. Hence, we obtain the distribution of the future state given a noisy measurement of the history,

$$P(x_{k+1}|y_{1:k+1}) \sim \mathcal{N}(\mu_{k+1}, P_{k+1})$$

and μ_{k+1} will be used to estimate the state x_{k+1}. We will refer this μ_{k+1} and P_{k+1} given by (4.1.4) as the 'Posterior' mean and covariance.

The Kalman filter algorithm can work for both linear and nonlinear dynamical models. However, a practical problem of implementing the Kalman filter to nonlinear model is computing the 'Forecast' covariance matrix P_f, since the formula (4.1.3) will not be valid. A common method to estimate the covariance matrix for a nonlinear model is using the Monte Carlo simulation. At each time step, multiple ensembles of x_k are drawn from its distribution:

$$\{x_k^i\} \sim P(x_k|y_{1:k}), \quad i = 1, 2, \cdots, N_e$$

where N_e is the total number of ensembles. Then by the law of large numbers, the 'forecast' mean and covariance at the next step can be approximated by

$$\begin{aligned} \bar{\mu}_f &= \frac{1}{N_e}\sum_{i=1}^{N_e} M(x_k^i) \\ \bar{P}_f &= \frac{1}{N_e - 1}\sum_{i=1}^{N_e}(M(x_k^i) - \bar{\mu}_f)(M(x_k^i) - \bar{\mu}_f)^T \end{aligned} \tag{4.1.5}$$

The Kalman filter using μ_f and P_f approximated by (4.1.5) will be referred to as the Ensemble Kalman filter [28].

When implementing the Kalman filter method to a stochastic dynamical model, we will use the root mean squared error (RMSE) and the Spread defined in (4.1.6) to examine the applicability of the algorithm.

$$\begin{aligned} \text{RMSE} &= (\frac{1}{n}\sum_{i=1}^{n}([x_k^t]_i - [x_k^a]_i)^2)^{\frac{1}{2}} \\ \text{Spread} &= (\frac{\text{Trace}(\text{P}_\text{k})}{n})^{\frac{1}{2}} \end{aligned} \tag{4.1.6}$$

where $[x_k^t]_i$ is the i^{th} component of the 'true' state x^t at time k, $[x_k^a]_i$ is the i^{th} component of the Kalman filter analysis state x^a at time k and P_k is the Kalman filter posterior covariance matrix at time k. By the its definition, RMSE can be viewed as the averaged error per variable of the predictor, while the Spread is approximating the average standard deviation of the predictor variable. In principle, the match of RMSE and Spread in scale is a signal that the Kalman filter algorithm is implemented appropriately.

4.1.2 Estimate the Multilayer Stochastic Model with Kalman Filter

In this section, we will implement the Ensemble Kalman filter method to the multilayer stochastic models (4.1.1) with different choices on the number L of truncated terms.

The data we are using to test the performance of the multilayer model is the synthetic data generated from Algorithm 1. The generated M_n^T is taken as the 'true' state of M_n and is used to evaluate the estimation errors. To simulate possible noises that may exist in a real measurement, we are randomly perturbing the 'true' state M_n^T by a small amount in fraction, and the perturbed quantities $\tilde{M}_n$ are used as the observation data in the Kalman filter algorithm. In particular, the data that is used to generate figures in this section is

$$\tilde{M}_n = (1 + 0.1 * \mathcal{N}(0,1))M_n^T \tag{4.1.7}$$

The initial states $M_0, M_1, \ldots, M_{L-1}$ and $\kappa_0, \kappa_1, \cdots, \kappa_{L-1}$ are generated through the following algorithms, in which M_0 is simulated from a random ρ_0 drawn from an uniform distribution, $M_1, \ldots, M_{L-1}$ are then generated from M_0 using the linear evaporation process, and $\kappa_0, \kappa_1, \cdots, \kappa_{L-1}$ are approximated by the values of $M_0, M_1, \ldots, M_{L-1}$. In fact, the initial values of $M_n's$ and $\kappa_n's$, when generated appropriately, won't affect the asymptotic behavior of the estimator when filtered by the Kalman filter algorithm.

Algorithm 2 Draw the intial states of $M_0, M_1, \ldots, M_{L-1}$

u = rand(I,1)
$v = u/(\frac{1}{I}\text{sum}(\text{u}))$
$M_0 = \frac{1}{I}\text{sum}(v)$
for $n = 1 : L-1$ **do**
  $\rho(n) = v \exp(-\tau n \omega)$
  $M(n) = \frac{1}{I}\text{sum}(\rho(n))$
end for

Algorithm 3 Draw the intial states of $\kappa_0, \kappa_1, \cdots, \kappa_{L-1}$

$\kappa_1 = 1$
$\kappa_2 = \kappa_1 + 1 + 0.3 * \mathcal{N}(0,1)$
for $n = 3 : L$ **do**
  $\kappa_n = \frac{1}{2}(\frac{M_{n-2}}{M_{n-2} - M_{n-1}} - \kappa_{n-1}) + \kappa_{n-1} + 1$
end for

As a comparison to all other estimators mentioned in Chapter 2, we first implement the Ensemble Kalman filter method to the multilayer stochastic model with the number of past M_i terms truncated at L=6. In our experiment, we take the ensemble size equal to 2000, which is large enough so that no inflation and localization is needed. To verify the Kalman filter algorithm is implemented appropriately in this case, we first look into the estimation RMSE and Spread, both of which are computed only for the variable M_n since the 'true' states of κ_n are unknown. The result

in Figure 4.1 shows a match of RMSE and Spread in scale, which indicates a reliable application of the Kalman filter to our model.

Algorithm 4 Kalman Filter implementation to the multilayer stochastic model

Ne=2000, H=[1,0]
for i=1:Ne **do**
  Draw $M^i_{1:L-1}$ from Algorithm 2
  Draw $\kappa^i_{1:L-1}$ from Algorithm 3
end for
for $n = L+1 : N$ **do**
  for $i = 1 : Ne$ **do**
    $\kappa^i_f = \kappa^i_{n-1} + 1 + 0.3 * \mathcal{N}(0,1)$
    $M^i_f = \sum_{j=1}^{6} h_j^{\kappa^j_f} M^i_{n-1}$
  end for
  Forecast: $\mu_f = [\frac{1}{Ne}\sum_{i=1}^{Ne} M^i_f; \frac{1}{Ne}\sum_{i=1}^{Ne} \kappa^i_f]$, P_f=Cov($[M_f; \kappa_f]$)
  $R = (0.1 * M^T_n)^2$
  $K = (P_f * H^T) * (H * P_f * H^T + R)^{-1}$
  $\mu_a = \mu_f + K * (M^T_n - H * \mu_f)$
  for $i = 1 : Ne$ **do**
    $[M^i_n, \kappa^i_n] = [M^i_f, \kappa^i_f] + K * (\tilde{M}_n + 0.1 * M^T_n * \mathcal{N}(0,1) - H * [M^i_f, \kappa^i_f])$
  end for
end for

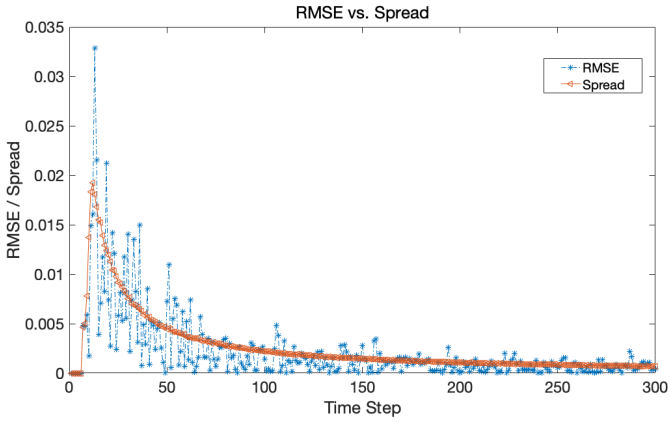

Figure 4.1: RMSE and Spread of the Kalman filter

We compare the relative one-step error $e_n = |\bar{M}_n - M^T_n|/M^T_n$ of the multilayer model implemented with the Kalman filter with those of the Empirical estimator, the

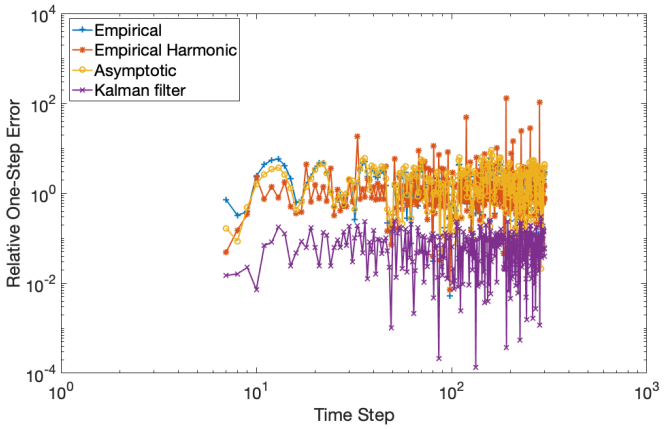

Figure 4.2: Relative One-Step error of Kalman filter and other estimators

Empirical harmonic estimator and the Asymptotic estimator in Figure 4.2. Among these different types of estimators, the multilayer model implemented with Kalman filter has the smallest relative one-step errors that are of order $O(10^{-2})$. The empirical linear estimator, which even though were seen to be one of the most reliable approaches when no-noisy data is available, is now suffering from the noises in the measurements. The relative one-step error of all three estimators except the multilayer model can be as large as $O(1)$.

This multilayer stochastic model using 6 M_n's in the past, when implemented with the Kalman filter method, is an improved way to estimate the states of the oil up to the time when noisy measurements are available. However, it is unstable to predict the future states without the help of data. In fact, since the linear operator associated with the parametrization truncated at $L = 6$ is not normal, none of these estimators using 6 past states are stable once the evolution trajectory of the past states exhibits random perturbation.

4.2 A Stable Multilayer Model With Tracking On Fewer History States

The multilayer reduced model (4.1.1) with 6 taps are proven to be reasonable when filtered by the Kalman algorithm using noisy measurement. However, it is unstable, meaning that the noise in the estimations of the history states will be amplified. This causes critical issues when we want to use the model to predict the future states of the oil, while no data from the future will be valid to apply the Kalman filter. A simple improvement on the stability is to use the same multilayer model (4.1.1) but with the choice of $L = 1$.

$$\bar{M}_n = h^{\kappa_n}\bar{M}_{n-1}, \quad h^{\kappa_n} = 1 - \frac{1}{2\kappa_n - 1} \tag{4.2.1}$$

Essentially, this estimator only makes use of the states in the latest past but discards all information from older time. Hence, despite its stability when used to predict the future, we will expect a sacrifice on accuracy thanks to the slow relaxation of the linear evaporation process.

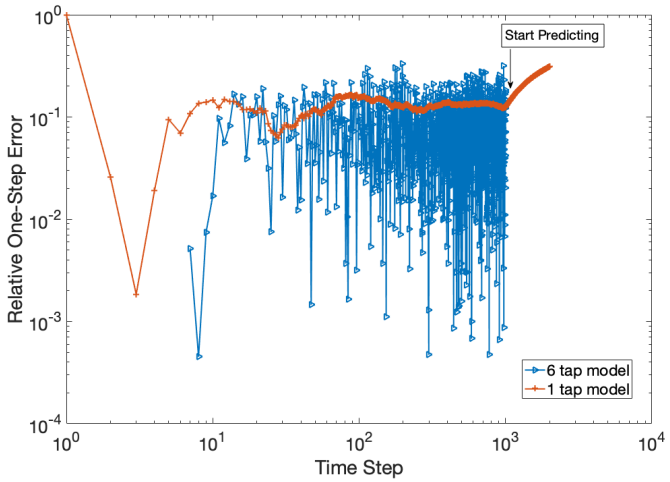

Figure 4.3: Relative One-Step error of multilayer reduced model with one tap

By Figure 4.3, the relative one-step error of the multilayer estimator with only one tap is at the order of $O(10^{-1})$ when filtered by the Kalman algorithm using noisy measurement (4.1.7), which is an order worse than the estimator with 6 taps. When being used to predict the future states, the multilayer estimator with one tap is stable, but the relative error can grow up to $O(1)$ in a few hundreds steps. We are seeking for an improvement of this one tap model on the estimation accuracy while still remaining its stability in the following way.

Instead of setting a one tap model for the entire average concentration M_n, we can track more details of the concentration evolution by splitting the entire domain of $\rho(\omega, t)$, $[0, 1]$ into K sub-domains, and building a one tap model for the average concentration ϕ_k on each small sub-domain. In particular, let's define

$$M(t) = \phi^1 + \phi^2 + \cdots + \phi^K \tag{4.2.2}$$

where

$$\phi^k = \int_{(k-1)/t}^{k/t} \rho(\omega, t)d\omega = \int_{(k-1)/t}^{k/t} \rho_0 e^{-\omega t}d\omega, \quad k = 1, 2, \ldots, K-1 \tag{4.2.3}$$

and

$$\phi^K = \int_{(K-1)/t}^{1} \rho(\omega, t) d\omega = \int_{(K-1)/t}^{1} \rho_0 e^{-\omega t} d\omega \tag{4.2.4}$$

To track the evolution of each 'bin' $\phi^k(t)$, we address a reduced model that only uses the history at the last time step, similar to model (4.2.1). However, since the boundaries of each sub-domain are time variant and the domain of ϕ^k at time n overlaps part of the domain of ϕ^{k-1} at time $n-1$, the past state of ϕ^{k-1} also contributes to the evolution of ϕ^k to the current state. Therefore, a non-autonomous discrete model that estimates the quantity for each 'bin' ϕ_k is

$$\begin{aligned} \phi_n^1 &= h_n^{(1,1)} \phi_{n-1}^1 \\ \phi_n^k &= h_n^{(k,k-1)} \phi_{n-1}^{k-1} + h_n^{(k,k)} \phi_{n-1}^k, \quad k = 2, 3, \ldots, K \end{aligned} \tag{4.2.5}$$

We will use the Yule-Walker equations again to determine the coefficients h's. To derive $h_n^{(k,k)}$, we have

$$\mathrm{E}[\phi_n^k \phi_{n-1}^k] = h_n^{(k,k-1)} \mathrm{E}[\phi_{n-1}^k \phi_{n-1}^{k-1}] + h_n^{(k,k)} \mathrm{E}[(\phi_{n-1}^k)^2] \tag{4.2.6}$$

$$\mathrm{E}[\phi_n^k] \mathrm{E}[\phi_{n-1}^k] = h_n^{(k,k-1)} \mathrm{E}[\phi_{n-1}^{k-1}] \mathrm{E}[\phi_{n-1}^k] + h_n^{(k,k)} (\mathrm{E}[\phi_{n-1}^k])^2 \tag{4.2.7}$$

Since ϕ_{n-1}^k and ϕ_{n-1}^{k-1} are independent, subtracting (4.2.7) from (4.2.6) yields

$$\begin{aligned} \mathrm{Cov}(\phi_n^k, \phi_{n-1}^k) &= h_n^{(k,k)} \mathrm{Var}(\phi_{n-1}^k) \\ \Rightarrow h_n^{(k,k)} &= \frac{\mathrm{Cov}(\phi_n^k, \phi_{n-1}^k)}{\mathrm{Var}(\phi_{n-1}^k)} \end{aligned} \tag{4.2.8}$$

Similarly, $h_n^{(k,k-1)}$ is derived using the equations:

$$\mathrm{E}[\phi_n^k \phi_{n-1}^{k-1}] = h_n^{(k,k-1)} \mathrm{E}[(\phi_{n-1}^{k-1})^2] + h_n^{(k,k)} \mathrm{E}[\phi_{n-1}^k \phi_{n-1}^{k-1}] \tag{4.2.9}$$

$$\mathrm{E}[\phi_n^k] \mathrm{E}[\phi_{n-1}^{k-1}] = h_n^{(k,k-1)} (\mathrm{E}[\phi_{n-1}^{k-1}])^2 + h_n^{(k,k)} \mathrm{E}[\phi_{n-1}^k] \mathrm{E}[\phi_{n-1}^{k-1}] \tag{4.2.10}$$

Subtracting (4.2.10) from (4.2.9) yields

$$h_n^{(k,k-1)} = \frac{\mathrm{Cov}(\phi_n^k, \phi_{n-1}^{k-1})}{\mathrm{Var}(\phi_{n-1}^{k-1})}$$

The variance and covariance can be computed in the manner of (2.2.38) and (2.2.39), resulting in

$$
\begin{aligned}
h_n^{(k,k)} &= \frac{2n-2}{2n-1} \cdot \frac{e^{-\frac{2n-1}{n-1}(k-1)} - e^{-\frac{2n-1}{n}k}}{e^{-2(k-1)} - e^{-2k}} \\
h_n^{(k,k-1)} &= \frac{2n-2}{2n-1} \cdot \frac{e^{-\frac{2n-1}{n}(k-1)} - e^{-\frac{2n-1}{n-1}(k-1)}}{e^{-2(k-2)} - e^{-2(k-1)}}
\end{aligned}
\tag{4.2.11}
$$

For $k = 1$, $h_n^{(1,1)} = (1 - \frac{1}{2n-1})$ so that the reduced model for ϕ^1 is the same as the asymptotic estimator (4.2.1) for M_n with one tap.

To make the estimators for ϕ_k autonomous, we use the same trick as being used in the multilayer stochastic model for M_n that introduces an additional dynamical variable κ that tracks the 'age' of the oil and recast the system into a larger phase. An autonomous multilayer reduced model for M_n using one tap and multiple 'bin's is

$$
\begin{aligned}
\phi_n^1 &= h_{\kappa_n}^{(1,1)} \phi_{n-1}^1 \\
\phi_n^k &= h_{\kappa_n}^{(k,k-1)} \phi_{n-1}^{k-1} + h_{\kappa_n}^{(k,k)} \phi_{n-1}^k, \quad k = 2, 3, \ldots, K \\
\kappa_n &= \kappa_{n-1} + 1 + s\theta_n^{'} \\
M_n &= \sum_{k=1}^{K} \phi_n^k
\end{aligned}
\tag{4.2.12}
$$

where h_{κ_n}'s are given by (4.2.11) with n repalced by κ_n. By making estimations for each component of M_n on smaller sub-domains, more details of the microscopic structure during its evolution are captured. Therefore, we should expect a more accurate estimation from this one tap multilayer estimator with multiple bins without loss of stability. Finally, one should get the high dimensional linear evaporation process (2.2.9) when taking the continuum limit of the model (4.2.5).

In Figure 4.4, we compare the relative one step errors of the 6 tap multilayer model, the one tap multilayer model, and the one tap 20 'bin's multiplayer model, all filtered by the Kalman filter algorithm using synthetic data generated from (4.1.7). Both one tap models are less sensitive to the measurement noise than the 6 tap model. The estimation errors of the one tap model with 20 bins are comparable to the 6 tap model on average, better than the original one tap model.

When being used to predict the future states of the oil, both one tap models are stable. However, the prediction errors are growing at a relatively fast rate even with the approaches using multiple 'bins', as Figure 4.5 shows. The limitation that the reduced models are poor at free predicting without data is due to the randomness of the linear evaporation of crude oil. Even with the same few past states, the evolution of crude oil due to evaporation could be different thanks to the difference in the microscopic structure. Thus, the reduced model in which only the total mass M_n is

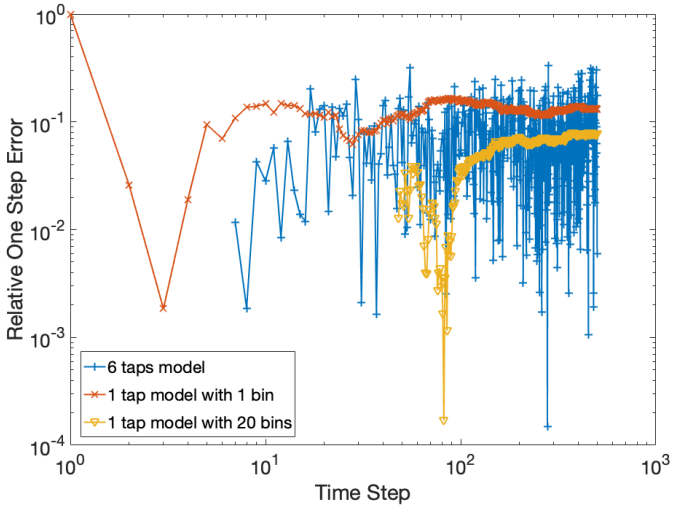

Figure 4.4: Relative One-Step error of one tap multilayer model with 20 bins

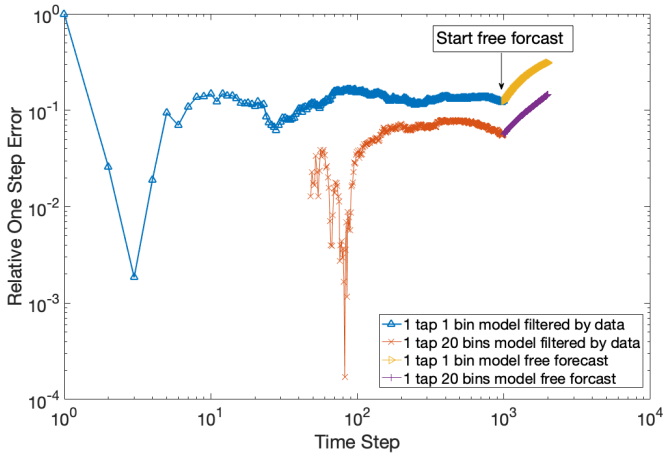

Figure 4.5: Free prediction errors of one tap multilayer model with 20 bins

tracked will not be able to reflect the evolution precisely without an incorporation of observational data.

To illustrate the randomness of the linear evaporation process, we simulate the variance of the stochastic process $M_n = \langle 1|\Lambda^n|\rho_0\rangle$ from 200 realizations generated from Algorithm 1 with all $M_0 = 1$ but random initial microscopic structure $|\rho_0\rangle$. We also compare the spread ($\sqrt{\text{Var}}$) of the linear evaporation process with the absolute one-step errors of the reduced models filtered by noisy data. Refer to Figure 4.6, the one-step errors of the estimations from both 1 tap reduced models are smaller than the process spread in a long term. While the estimations from the 1 tap model with 20 bins are better than the process spread even in a shorter period of time.

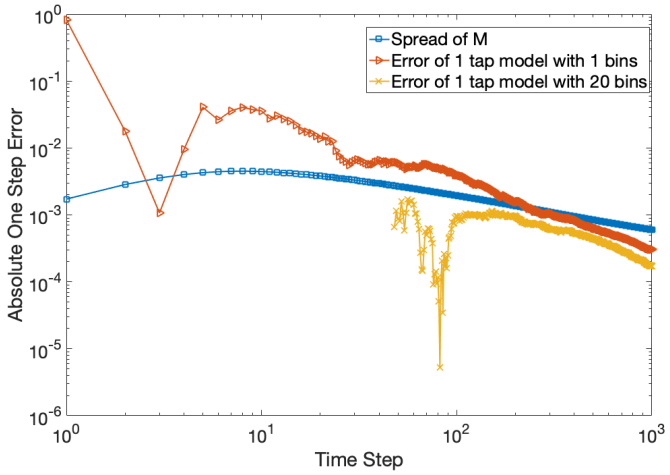

Figure 4.6: Prediction errors of one tap multilayer

Therefore, the reduced 1 tap model with multiple bins is reliable on estimating the current states of the oil using observational data and is stable to predict the future evolution without data. However, its accuracy in prediction is limited due to the lack of information about the microscopic structure.

Chapter 5

Conclusions and Future Research Directions

In this dissertation, we have studied the phenomena of oil spreading on water surface. We address a reduced model that captures the local dynamics of an oil slick spreading on flowing water surface and present analysis for different scenarios. When the underlying water is locally steady, a full PDE model is analyzed to yield that the oil slick radius is expanding at a rate proportional to $t^{\frac{3}{8}}$ with the velocity of the slick equals $\frac{3}{8}\frac{x}{t}$. For spreading on a water surface where the flow is locally contracting towards the center of the oil slick, a stationary state is found for the oil slick. For an oil slick spreading on a water surface where the flow is locally expanding towards the edge the slick, the slick has an exponential spreading rate whose exponent is equal to the free stream rate. A quasi-steady state is found in this case. We also develop numerical schemes that simulate the dynamics of an oil slick spreading on steady water surface and surface with expanding water flow.

For modeling the evolution of crude oil, we introduce a dimension reduction for systems with slow relaxation and develop a multilayer stochastic model. Using the multilayer reduced model, we are able to estimate a single observable quantity of oil based on its past states, without further knowledge on the microscopic structure inside the crude oil. Through synthetic data experiments, our reduced model is demonstrated to have an improved accuracy when implemented with data assimilation methods and can maintain stability while predicting a future state when no data is available.

For future work on this topic, we will expect to investigate on the effects of other physical processes that may have impact on the spreading of oil on the sea surface, but have not been considered in the models developed in this thesis. As an example, when modeling the oil spill process on the sea, the effect of oceanic flows must be taken into account. Unlike the unidirectional flows that we assume in section 3.1, the oceanic waves are more complicated and involve more physical effects. On a small length scale, the oceanic waves almost have a periodic propagation. One of the significant effects on a particle flowing with such periodic waves is Stokes drift.

In general, Stokes drift reflects the difference in end position when tracing a parcel as it travels with the fluid flows after a predefined amount of time (usually one wave period). The Stokes drift velocity is the average velocity of the parcel during the defined period. For water waves, George Gabriel Stokes first formulated the Stokes drift in 1847. For instance, let's consider the case of infinite-deep water, with linear wave propagation of a sinusoidal wave on a free surface of a fluid layer:

Figure 5.1: Illustration of nearshore oil layer floating on water. Captured from [23]

$$\eta = a\cos(kx - \omega t) \tag{5.0.1}$$

where η is the elevation of the free surface in the vertical direction; a is the wave amplitude; k is the wave number; ω is the angular frequency; λ is the wave length; T is the wave period; x is the horizontal coordinate and the wave propagation direction; z is the vertical coordinate. Then it can be derived that the horizontal component $u_S(z)$ of the Stokes drift velocity for deep-water waves is approximately [21]

$$u_S(z) \approx \omega k a^2 e^{2kz} = \frac{4\pi^2 a^2}{\lambda T} e^{\frac{4\pi z}{\lambda}} \tag{5.0.2}$$

Such a drift effect from the oceanic waves could have impact on the oil spreading and should not be neglected. Restrepo, Venkataramani and Dawson develops a model that explains the effect of the Stokes drift and the non-uniform dispersion in the vertical direction on the parking of buoyant pollutants in the nearshore in 2014 [23].

In particular, let's look at a scenario of oil transport in the nearshore. A simple illustration is shown in Figure 10, in which the quiescent ocean level is at $z = 0$, the basin is bounded below at $z = -H(x)$. The oil in the surface slick may be entrained by the action of wave breaking and turbulent mixing. In most general cases, the floating oil can be treated as two stratification. A very thin layer of pure oil riding on the ocean surface will be referred as the oil slick. Immediately below the oil slick layer, oil bulks are found in suspension in a layer of ocean. We will refer this portion of oil as the interior oil. Let $h(x,t)$ denote the thickness of the oil slick layer and assume that the ocean layer containing the suspended oil has the maximum depth P. B denotes the dimensionless volume fraction of the oil in suspension. Also a function $b(x;t)$ is introduced to represent the thickness of an 'equivalent' pure oil layer containing the same amount of oil as in the interior.

The oil slick is moving with the water surface, pushed by the wave propagation. In a rough sense, one can approximate the cross-shore component of the oil slick velocity u_S by $U^{St}(x,0;t) := \mathcal{U}^{St}$, the Stokes drift velocity evaluated at the surface. Assume that the oil slick and the interior oil have the same viscosity $D(X)$ so that a diffusive flux on the surface is $-D(x)\frac{\partial h}{\partial x}$ and in the suspension bulk is $-D(X)\frac{\partial b}{\partial x}$.

Lastly, the exchange of material between the surface and the bulk due to wave-mixing and buoyancy can be characterized on a long time scale corresponding to averaging over many waves. The net flux from the slick into the suspension layer is modeled as a linear expression $\frac{1}{\tau(x)}((1-\gamma)h - \gamma PB)$, where $\gamma \in (0,1)$ is a parameter that sets the relative proportions of the oil in the slick and in suspension for vertical equilibrium, i,e,

$$\frac{h}{PB} = \frac{\gamma}{1-\gamma}$$

$\tau(x)$ is the time scale for the vertical mixing.

Then a full PDE model that describes the transport of the floating oil in the nearshore is derived as:

$$\frac{\partial h}{\partial t} + \frac{\partial [u_S(x)h]}{\partial x} = -\frac{(1-\gamma)h - \gamma PB}{\tau(x)} + \frac{\partial}{\partial x}[D(x)\frac{\partial h}{\partial x}] \tag{5.0.3}$$

$$\frac{\partial b}{\partial t} + \frac{\partial [v(x)b]}{\partial x} = \frac{(1-\gamma)h - \gamma PB)}{\tau(x)} + \frac{\partial}{\partial x}[D(x)\frac{\partial b}{\partial x}] \tag{5.0.4}$$

with zero flux conditions at the boundary $x = 0$ and $x = L$:

$$\begin{aligned} u_S(x)h - D(x)\frac{\partial h}{\partial x} &= 0, \quad x = 0, L \\ v(x)b - D(x)\frac{\partial b}{\partial x} &= 0, \quad x = 0, L \end{aligned} \tag{5.0.5}$$

This model reflects several main physical effects involved in the oil transport in the nearshore ocean, including (1) A mean advective flow that is depth dependent and is shore directed on the surface, (2) A dispersion model that models the transport due to the fluctuating component of the velocity and accounts for the enhanced diffusion in the break zone, (3) A simplified oil model that includes the effects of buoyant stratification of the oil into a surface slick and a suspending bulk, and (4) An vertical exchange interaction between the suspending bulk oil and the surface oil slick. With specified initial conditions $h(x;0)$ and $b(x;0)$, one can solve this complete PDE model numerically. And through a model reduction, it has been shown that the results obtained from the full PDE model are robust and depend only on gross feature of the diffusive parameter $D(x)$ and the vertical mixing time $\tau(x)$, but not on the details of these functions [23]. Therefore, simple choices on the functions D and τ can still yield useful results for real physical flows in nature.

However, in this model, a simplification for modeling the advection flow is assuming that $u_S \approx U^{St}(x,0;t)$, which does not distinguish the horizontal moving velocity of the oil from the velocity of the water. This flaw can be potentially improved by the solution we present in section 2.4 and 3.1, in which a distinguished horizontal velocity of the oil slick can be estimated numerically while the slick is sliding over a

steady water surface, or over a flowing water surface with expanding or contracting stream. For real oceanic waves, which usually generate periodic streams on a small scale, it is promising to simulate its effect on the moving velocity of a floating oil slick by splitting the entire domain into small regions, each has unidirectional stream, and evaluating the local moving velocity of the oil through our analysis of in Chapter 3.

Nevertheless, there are other effects that may have influence on the oil spreading process but not been taken into account in our calculation, nor in the nearshore model developed in [23]. The driving effect from the wind right above the water surface has significant impact to promote or retard the oil slick's growing and should not be neglected. Korinenko [17] conducts a field study of film spreading on a sea surface through experiments. The experiments were carried out in the coastal zone of the Black Sea in a wide range of wind speeds and wave conditions. Vegetable oil was used for preparing the surfactants. The experimental results find that at moderate and strong wind speeds, the slicks take on a shape similar to an ellipse and are orientated in the direction of the air flow. Hoult [14] estimates that with a wind velocity above the water surface a certain distance (usually 10 meters), the drift water velocity by the wind is approximately

$$U_{water} = [\frac{\rho_{air}}{\rho_{water}}]^{1/2} U_{wind} = 0.035 U_{wind} \tag{5.0.6}$$

This result can be verified by laboratory studies [13, 19], and field observations [24, 16]. However, no further study has been conducted on the wind drift velocity of a more viscous fluid like oil.

Also we should address the additional difficulty that arises in modeling the oil spill in large scale. When a massive amount of oil spills, it will spread to a large area after some time. The characteristic length of the oil layer after a few days from spilling occurs could be thousands of miles. In such a large-scale phenomenon, the rotation of earth is normally playing an important role so that the effect of the Coriolis force must be considered. Maderich [18] examines the effect of the Coriolis force on the oil spill spreading in the gravity-viscous regime. They describe a new shallow water model for the transport and spreading of oil slick of arbitrary shape, in which the Coriolis force is included in the momentum equations and the oil-water friction is parameterized in a frame of the boundary layer theory including the Ekman friction.

The process of oil spreading on the sea is complicated. There are numerous studies on this phenomena, but typically only a few effects are incorporated into the models. Developing a comprehensive mathematical model that incorporates effect from every physical process involved in the oil spread evolution on the sea is challenging. With the rapid progress in the field of data science, statistical methods that absorb observable data from the real world can be promising complement tools to help people understand this process better.

References

[1] SN Brown and K Stewartson. On similarity solutions of the boundary-layer equations with algebraic decay. *Journal of Fluid Mechanics*, 23(04):673–687, 1965.

[2] J Buckmaster. Viscous–gravity spreading of an oil slick. *Journal of Fluid Mechanics*, 59(03):481–491, 1973.

[3] Rachid Chebbi. Dynamics of unidirectional gravity-inertial spreading of oil on water. *Chemical engineering science*, 60(23):6806–6813, 2005.

[4] Rachid Chebbi, Sami A Abd Elrahman, and Hassan K Ahmed. Experimental study of unidirectional viscous-gravity spreading of oil on water. *Journal of chemical engineering of Japan*, 35(12):1330–1334, 2002.

[5] R. Courant, K. Friedrichs, and H. Lewy. On the partial difference equations of mathematical physics. *IBM J. Res. Dev.*, 11(2):215–234, March 1967.

[6] J. Crank and P. Nicolson. A practical method for numerical evaluation of solutions of partial differential equations of the heat-conduction type. *Mathematical Proceedings of the Cambridge Philosophical Society*, 43(1):5067, 1947.

[7] P. DuChateau and D. Zachmann. *Applied Partial Differential Equations*. Dover Publications, Inc, 2002.

[8] James A Fay. The spread of oil slicks on a calm sea. In *Oil on the Sea*, pages 53–63. Springer, 1969.

[9] James A Fay. Physical processes in the spread of oil on a water surface. In *International Oil Spill Conference*, volume 1971, pages 463–467. American Petroleum Institute, 1971.

[10] P. Flajolet and A. Odlyzko. Singularity analysis of generating functions. *SIAM Journal on Discrete Mathematics*, 3(2):216–240, 1990.

[11] Mediterranean Decision Support System for Marine Safety. Marine pollution. `www.medess4ms.eu/marine-pollution`, 2012.

[12] Schlichting Hermann et al. *Boundary layer theory*. McGraw-Hill, 1979.

[13] George M Hidy and Erich J Plate. Wind action on water standing in a laboratory channel. *Journal of Fluid Mechanics*, 26(04):651–687, 1966.

[14] David P Hoult. Oil spreading on the sea. *Annual Review of Fluid Mechanics*, 4(1):341–368, 1972.

[15] David Parks Hoult and Walter Suchon. *The spread of oil in a channel*. Massachusetts Institute of Technology, Department of Mechanical Engineering, 1970.

[16] P Hughes. A determination of the relation between wind and sea-surface drift. *Quarterly Journal of the Royal Meteorological Society*, 82(354):494–502, 1956.

[17] Aleksandr E Korinenko and Vladimir V Malinovsky. Field study of film spreading on a sea surface. *Oceanologia*, 56(3):461–475, 2014.

[18] Vladimir Maderich, Igor Brovchenko, and Kyung Tae Jung. Oil spreading in instantaneous and continuous spills on rotating earth. *Environmental fluid mechanics*, 12(4):361–378, 2012.

[19] JA O'brien. Wind tunnel experiments on oil slick transport. *Journal of hydraulic Research*, 9(2):197–215, 1971.

[20] S. Patankar. *Numerical Heat Transfer and Fluid Flow*. CRC Press, first edition, 1980.

[21] O.M. Phillips. *The dynamics of the upper ocean*. Cambridge University Press, 1977.

[22] G. Polya and G. Szego. *Problems and Theorems in Analysis*. Springer, Berlin, Heidelberg, 1998.

[23] Juan M Restrepo, Shankar C Venkataramani, and Clint Dawson. Nearshore sticky waters. *Ocean Modelling*, 80:49–58, 2014.

[24] James E Smith. Torry canyon pollution and marine life. 1968.

[25] Robert Middleton Terrill. Laminar boundary-layer flow near separation with and without suction. *Philosophical Transactions of the Royal Society of London A: Mathematical, Physical and Engineering Sciences*, 253(1022):55–100, 1960.

[26] J.W. Thomas. *Numerical Partial Differential Equations: Finite Difference Methods*. Springer-Verlag New York, first edition, 1995.

[27] Shankar C. Venkataramani, Raman C. Venkataramani, and Juan M. Restrepo. Dimension reduction for systems with slow relaxation. *Journal of Statistical Physics*, 167(3):892–933, May 2017.

[28] P. Zarchan and H. Musoff. *Fundamentals of Kalman Filtering: A Practical Approach*. Reston, VA : American Institute of Aeronautics and Astronautics, fourth edition, 2015.